Ligand-independent activity of the ghrelin receptor modulates AMPA receptor trafficking and supports memory formation

Luís F. Ribeiro[1,*,#,&], Tatiana Catarino[1,2,*], Mário Carvalho[1,3,*], Luísa Cortes[1,2], Sandra D. Santos[1,2], Patricio O. Opazo[4,5,§], Lyn Rosenbrier Ribeiro[6,%], Bárbara Oliveiros[7,8],Daniel Choquet[4,5,9], José A. Esteban[10], João Peça[1,11], Ana Luísa Carvalho[1,11,&]

[1]CNC-Center for Neuroscience and Cell Biology, University of Coimbra, 3004-504 Coimbra, Portugal.

[2]University of Coimbra, IIIUC- Institute for Interdisciplinary Research, 3030-789 Coimbra, Portugal

[3]MIT-Portugal Bioengineering Systems Doctoral Program

[4]University of Bordeaux, Interdisciplinary Institute for Neuroscience, UMR 5297, 33000 Bordeaux, France.

[5]CNRS, UMR 5297, 33000 Bordeaux, France.

[6]Functional and Mechanistic Safety, Clinical Pharmacology and Safety Sciences, R&D AstraZeneca, Cambridge, CB2 0SL, United Kingdom.

[7]Laboratory of Biostatistics and Medical Informatics (LBIM), Faculty of Medicine, University of Coimbra, 3000-548 Coimbra, Portugal.

[8]Coimbra Institute for Clinical and Biomedical Research (iCBR), Faculty of Medicine, University of Coimbra, 3000-548 Coimbra, Portugal.

[9]Bordeaux Imaging Center, UMS 3420, CNRS-Bordeaux University, US4 INSERM, 33000 Bordeaux, France.

[10]Department of Molecular Neurobiology, Centro de Biología Molecular "Severo Ochoa", Consejo Superior de Investigaciones Científicas (CSIC) / Universidad Autónoma de Madrid, 28049 Madrid, Spain.

[11]University of Coimbra, Department of Life Sciences, 3000-456 Coimbra, Portugal.

*These authors contributed equally to this work.

#Current address: VIB Center for Brain and Disease Research, Leuven, Belgium; KU Leuven Department of Neurosciences, Leuven, Belgium.

§Current address: Clem Jones Centre for Ageing Dementia Research, Queensland Brain Institute, University of Queensland, St. Lucia, Queensland, Australia.

%Current address: Medicines Discovery Catapult, Block 35, Mereside, Alderley Park, Alderley Edge, Macclesfield, SK10 4TG, United Kingdom.

&Corresponding author. Email: luis.ribeiro@kuleuven.vib.be (LFR); alc@cnc.uc.pt (ALC).

Abstract

The ability of animals to store and retrieve food caches in the wild requires the integration of biological signals of hunger, satiety and memory. The role of ghrelin in regulating feeding and memory makes ghrelin receptors an important target to shape the required cellular and molecular responses. We investigated the effects of the high ligand-independent activity of the ghrelin receptor GHS-R1a on the physiology of excitatory synapses in the hippocampus. Blocking this type of activity produced a decrease in the synaptic content of AMPA receptors in hippocampal neurons and a reduction in GluA1 phosphorylation at serine residue 845. Reduced ligand-independent activity from GHS-R1a increased surface diffusion of AMPA receptors and impaired AMPA receptors synaptic delivery mediated by chemical long-term potentiation. These observations support a role for the ligand-independent activity of GHS-R1a in regulating AMPA receptors trafficking under basal conditions and synaptic plasticity. Accordingly, we found that blocking the ligand-independent GHS-R1a activity impairs spatial and recognition memory.

Introduction

Ghrelin is a peptide hormone believed to signal meal initiation (*1, 2*) and is found at the highest concentration in human plasma immediately before each meal (*3*). It is mainly secreted by X/A-like cells in the oxyntic glands of the stomach and intestine (*4*). Apart from effects on food intake (*5*) and feeding behavior (*6, 7*), ghrelin influences several other physiological systems (*8*). For example, it is well established that ghrelin improves learning and memory (*9, 10*), facilitates reward through its action on the mesolimbic dopamine system (*11*), modulates anxiety-like (*9*) and depressive-like (*12*) behaviors, and enhances long-term fear memory (*13*).

The actions of ghrelin are mediated by the growth hormone secretagogue receptor type 1a (GHS-R1a), a G protein-coupled receptor (GPCR), whose activation by ghrelin regulates gene expression, neuronal excitability and AMPA (α-amino-3-hydroxy-5-methyl-4-isoxazolepropionic acid)-type glutamate receptors (AMPARs) trafficking (*10, 14-16*). In the brain, GHS-R1a is highly expressed in the hypothalamus, pituitary gland and hippocampus (*17*) and its expression levels increase during fasting (*18-20*). Notably, GHS-R1a displays unusually high constitutive activity, corresponding to approximately 50% of its maximal activity (*21*), which results from a natural shift in the equilibrium between its inactive and active conformations (*22*), in the absence of ligand. The ligand-independent GHS-R1a activity plays a role in the control of food intake and regulation of body weight (*18, 20, 23-25*), and in the acquisition of conditioned taste aversion (*26*). Human mutations that lead to a selective loss of constitutive activity of GHS-R1a, but that do not interfere with ghrelin-induced activation, are associated with familial short stature (*27-30*). A study in mice expressing a human mutation in the GHSR that impairs constitutive GHSR activity revealed that this activity contributes to the native depolarizing conductance of hypothalamic neurons, and to growth hormone release (*31*). The recently described liver-expressed antimicrobial peptide 2 (LEAP2) is an endogenous antagonist of GHS-R1a (*32*), which also exhibits inverse agonist activity, blocking the ligand-

independent activity of GHS-R1a (*33, 34*). LEAP2 plasmatic levels are lower in fasted states (*32, 33*), increase with body mass and blood glucose, and are higher in obesity (*33*), in a manner that is opposite to that of plasma acyl-ghrelin. These observations indicate that acyl-ghrelin and LEAP2 bidirectionally control ligand-dependent activity of GHS-R1a, and importantly that LEAP2 might exert endogenous control of the ligand-independent activity of GHS-R1a, which is physiologically relevant (*35*).

GHS-R1a knock-out (KO) animals display spatial and contextual memory impairments (*36, 37*), which can be attributed to the absence of ghrelin-triggered effects, but also to the loss of the ligand-independent activity. However, the physiological importance of GHS-R1a constitutive activity for learning and memory has not been described. Here, using a combination of imaging, biochemical and electrophysiological approaches, and behavior analysis, we uncover a role for the ligand-independent activity of GHS-R1a in providing tonic control for the regulation of AMPARs trafficking, influencing synaptic plasticity in the hippocampus and interfering with learning and memory in vivo. These findings should be taken into account given inverse agonists of GHS-R1a that are presently being tested in humans to treat alcohol use disorder (*38, 39*).

Results

Ligand-independent activity of GHS-R1a in hippocampal neurons

In the absence of ligand, GHS-R1a displays unusually high constitutive activity (*21*), which has been shown to control food intake and body weight (*18, 20, 23-25*), and the acquisition of conditioned taste aversion (*26*). Since the activity of GHS-R1a in the absence of agonist has been associated with the G_q protein/phospholipase C (PLC)/inositol-3,4,5-triphosphate (IP_3) pathway (*21*), to directly evaluate the ligand-independent activity of GHS-R1a in hippocampal neurons we visualized PLC activation

using a construct consisting of the PLCδ pleckstrin homology domain (PLCδPH) fused to GFP (PLCδPH-GFP), as previously described (*40*). PLCδPH-GFP favors phosphatidylinositol 4,5-bisphosphate (PIP$_2$) over other inositol phospholipids, but has higher affinity for IP$_3$ than for PIP$_2$ (*41*). Therefore, PIP$_2$ hydrolysis by PLC causes PLCδPH-GFP to translocate from the plasma membrane to the cytosol, where it binds respectively to PIP$_2$ or IP$_3$. Under basal conditions, PLCδPH-GFP is localized at the plasma membrane and along the dendritic shaft in primary cultured hippocampal neurons (Fig. 1, A and B; *t0*). Acute bath application of the nonpeptidyl GHS-R1a agonist MK-0677 caused a robust translocation of PLCδPH-GFP into the cytosol (F/F0 = 1.33±0.16; Fig. 1, A and C, and Movie S1), reflecting the generation of IP$_3$, and which was accompanied by a decrease in the plasma membrane levels of the probe (F/F0 = 0.78±0.03; Fig. 1, A and C, and Movie S1). These observations show activation of GHS-R1a-mediated signaling by the receptor agonist in hippocampal neurons. To evaluate the basal constitutive signaling of GHS-R1a, we first used [D-Arg[1],D-Phe[5],D-Trp[7,9],Leu[11]]-substance P (SP-A), a well-established GHS-R1a inverse agonist (*20, 21*), to block the receptor ligand-independent activity. Acute application of SP-A led to an increase in the plasma membrane levels of PLCδPH-GFP (F/F0 = 1.19±0.06), with no detectable changes in the cytoplasmatic fluorescent signal (F/F0 = 1.06±0.02; Fig. 1, B and C, and Movie S2). To evaluate the long-term effect of the ligand-independent activity of GHS-R1a, we blocked it in PLCδPH-GFP-transfected hippocampal neurons for 20 h with either SP-A or with a recently described blood-brain barrier (BBB) permeable inverse agonist of GHS-R1a, AZ12861903 (AZ), which decreases the ligand-independent activity of the receptor (*25*). Neurons were fixed and the spine and dendritic shaft distribution of PLCδPH-GFP was evaluated (Fig. 1, D and E). We observed that in neurons treated with either of the GHS-R1A inverse agonists, SP-A or AZ, there was a redistribution of PLCδPH-GFP from the dendritic shaft to spines (Fig. 1, D and E), suggestive of spine accumulation of PIP$_2$. These results indicate that the basal GHS-R1a activity in the absence of the ligand contributes to baseline hydrolysis of PIP$_2$, which is

blocked by SP-A and AZ, and support ligand-independent activity of GHS-R1a in hippocampal neurons.

AMPA receptors surface and synaptic localization is regulated by ligand-independent activity of GHS-R1a

To test whether the ligand-independent activity of GHS-R1a could provide a tonic signal in the hippocampus and regulate AMPARs trafficking, we evaluated whether inverse agonists of GHS-R1a affect the synaptic content of AMPARs in cultured hippocampal neurons. Incubation of 15 days in vitro (DIV) hippocampal neurons with either SP-A or AZ decreased the total cell surface levels of GluA1 and the levels of cell surface GluA1-containing AMPARs co-localized with the postsynaptic protein PSD95 and the presynaptic protein VGluT1 (Fig. 2, A to D). In contrast, incubation with GHS-R1a antagonist JMV2959 did not significantly affect the total or synaptic levels of surface GluA1 (fig. S1, A and B). Similarly to GluA1, GluA2 synaptic levels were decreased in neurons incubated with SP-A (Fig. 2, E and F). However, the incubation with SP-A did not affect synapse density in 15 DIV cultured hippocampal neurons (fig. S1C), measured by the colocalization of PSD95 and VGluT1 puncta. SP-A also decreased the total surface and synaptic levels of GluA1, as well as synapse density in older neurons (20 DIV; Fig. 2, G and H, and fig. S1C), but not in 7 DIV neurons (Fig. 2, I and J, and fig. S1C), which at this age present lower expression levels of GHS-R1a (*15*).

To test whether the ligand-independent activity of GHS-R1a functionally modulates CA3-CA1 hippocampal excitatory transmission, organotypic hippocampal slices were treated with SP-A for 20 h, and electrophysiological recordings were performed. The AMPA/NMDA ratio of synaptic responses decreased significantly after treatment with SP-A, compared with control neurons, whereas GHS-R1a antagonist [D-Lys^3]-GHRP-6 did not affect AMPA/NMDA ratios (Fig. 2, K and L), in agreement with low levels of ghrelin in the culture, and a specific role for the GHS-R1a inverse agonist in

inhibiting CA3-CA1 synaptic transmission. Together, these results suggest that the ligand-independent activity of GHS-R1a regulates AMPARs levels and excitatory synaptic transmission under basal conditions.

We then silenced the expression of GHS-R1a in cultured hippocampal neurons using a short hairpin RNA (shRNA) containing a previously validated sequence (*42*) and tested for surface levels of GluA1. Knock-down of GHS-R1a decreased the levels of surface and synaptic GluA1, which were rescued when the shRNA was co-expressed with an shRNA-insensitive human form of the receptor (hGHS-R1a; Fig. 3, A to C). Notably, treatment with either SP-A or AZ did not affect the total surface or synaptic levels of GluA1 in neurons where the expression of GHS-R1a was silenced (Fig. 3, A to C), confirming the specificity of SP-A and AZ in targeting the GHS-R1a. We have also tested whether a mutant form of GHS-R1a which lacks ligand-independent activity can rescue the phenotype found in neurons depleted for GHS-R1a. We have used GHS-R1a F279L, a mutant form of the GHS-R1a that was identified in a child with short stature (*30*). Phe[279] in GHS-R1a was found to be critical for the constitutive signaling activity of the receptor (*43*). Whereas reintroduction of wild-type (WT) GHS-R1a rescued normal synaptic levels of GluA1 in neurons depleted of endogenous GHS-R1a, expression of GHS-R1a F279L did not (Fig. 3, D and E). These observations confirm the idea that the ligand-independent activity of GHS-R1a regulates baseline synaptic levels of AMPA receptors.

Ligand-independent GHS-R1a activity controls its ligand-dependent effect on AMPA receptors surface and synaptic localization

Since the ligand-independent activation of GHS-R1a promotes its own basal internalization (*44*), we reasoned that it could limit the agonist-induced effects in the hippocampus (*15*). To test this, we used 15 DIV cultured hippocampal neurons, for which no effect of ligand-dependent activation of GHS-R1a on AMPARs surface expression

was detected (Fig. 4, A and B). We found that upon blockade of the ligand-independent GHS-R1a activity with SP-A, subsequent activation of GHS-R1a with the agonist MK-0677 increased the surface and synaptic expression of GluA1-containing AMPARs (Fig. 4). Together, these observations indicate that the hippocampal ligand-independent GHS-R1a activity promotes tonic expression of synaptic AMPARs (Figs. 2 and 3), and on the other hand limits the agonist-mediated effects of GHS-R1a on AMPARs trafficking (Fig. 4).

Ligand-independent activity of GHS-R1a regulates AMPA receptors surface mobility

To determine how the ligand-independent activity of GHS-R1a may regulate AMPARs, we tested for effects on the cell surface diffusion of GluA1 AMPARs subunit. We expressed super ecliptic pHluorin (SEP)-GluA1 in cultured hippocampal neurons and took advantage of the single particle tracking approach to monitor individual AMPARs complexes (Fig. 5, A to E). Hippocampal neurons were exposed to SP-A for 1 hour and single particle imaging of SEP-GluA1 was performed thereafter. SP-A exposure significantly increased the surface diffusion of GluA1 (both the mean square displacement and diffusion coefficient were increased; Fig. 5, A and B), decreased the fraction of synaptic immobile receptors (Fig. 5C) and decreased the synaptic residence time of GluA1-containing AMPARs (Fig. 5D).

We repeated this experiment now applying AZ and using quantum-dots labeled antibodies against an extracellular region in GluA1, to follow endogenous AMPARs (Fig. 5, F to J). Endogenous GluA1 also showed increased mean square displacement and diffusion coefficient and decreased synaptic residence time in neurons treated with AZ. Similarly, SP-A treatment increased the surface diffusion of endogenous GluA2 (fig. S2, A to D). These observations provide evidence that the ligand-independent activity of GHS-R1a contributes to decrease the surface diffusion of synaptic AMPARs, thereby

increasing the synaptic content of AMPARs under basal conditions in hippocampal neurons.

Effects of ligand-independent activity of GHS-R1a on activity-induced synaptic incorporation of AMPA receptors

We then assessed whether activity-induced synaptic incorporation of AMPARs is regulated by the ligand-independent activity of GHS-R1a. We used a neuronal culture model of chemical long-term potentiation (cLTP), in which activation of NMDA receptors triggers an increase in the expression of surface and synaptic AMPARs (*45*). In agreement with previous reports, application of glycine (co-agonist of NMDA receptors), in the absence of Mg^{2+}, led to a significant increase in the synaptic expression of GluA1-containing AMPARs compared to control cells (Fig. 5, K to N). However, this effect was blocked in neurons pre-incubated with either SP-A (Fig. 5, K and L) or AZ (Fig. 5, M and N), indicating that the ligand-independent GHS-R1a activity is necessary for AMPARs synaptic insertion upon cLTP.

Intracellular signaling of hippocampal ligand-independent GHS-R1a activity.

We tested cell signaling pathways downstream of the ligand-independent GHS-R1a activity that could result in altered trafficking of AMPARs. We found that upon blockade of the ligand-independent activity of GHS-R1a in organotypic hippocampal slices there was a decrease in the phosphorylation of GluA1 at serine 845 (Ser^{845}) (Fig. 6A), a PKA phosphorylation site critical for priming AMPARs for synaptic insertion (*46*). Additionally, a decrease in the phosphorylation of CaMKIV (Fig. 6B) was detected, whereas no changes were found in the phosphorylation of GluA1 at serine 831 (Ser^{831}), in the phosphorylation of stargazin or in the phosphorylation of Akt (Fig. 6, C to E). These results suggest that PKA activation downstream of the ligand-independent activity of

GHS-R1a may result in phosphorylation of GluA1 at Ser[845] and contribute to maintaining a population of AMPARs available for synaptic insertion.

To test whether the ligand-independent GHS-R1a activity contributes to AMPARs trafficking through effects on GluA1 phosphorylation at Ser[845], we evaluated whether SP-A affects the cell surface and synaptic levels of phosphodead and phosphomimetic mutants of GluA1 at Ser[845] (S845A and S845D, respectively). We found that contrarily to WT GluA1, SP-A treatment did not alter the cell surface or synaptic levels of either of these mutants (Fig. 6, F and G), suggesting GluA1 phosphorylation at Ser[845] as one mechanism through which the ligand-independent activity of GHS-R1a regulates AMPARs trafficking.

Ligand-independent activity of GHS-R1a is relevant for memory formation

Given the role of the hippocampus and excitatory transmission in spatial memory (*47*), and that GHS-R1a KO mice present memory impairments (*36, 37*), we tested whether the ligand-independent activity of GHS-R1a plays a role in memory formation by evaluating performance in the novel object recognition test (*48*) in mice injected with the BBB-permeable inverse agonist of GHS-R1a AZ. During the familiarization session, animals were allowed to explore two identical objects for 10 min. After 6 hours, one of the objects was replaced with a novel object, and the percentage of time exploring either object was measured (test session, Fig. 7A). Whereas control animals explored the novel object a higher number of times and for longer, animals treated with the GHS-R1a inverse agonist prior to the familiarization session did not show a preference for either object, as measured by the number of explorations of each object (Fig. 7B) or time spent with each object (Fig. 7C).

To test whether the ligand-independent activity of GHS-R1a is relevant for spatial memory, we used the object displacement test (*49*) (Fig. 7D). During the habituation

session the animals explored an open-field arena in the absence of objects for 6 min; immediately after, the animals were treated with GHS-R1a inverse agonist or vehicle injection. The animals returned to the open-field 10 min post-injection, and 2 different objects were present in specific locations. This familiarization session lasted 6 min and was repeated twice. After 24 hours, the animals were tested in the open-field with one of the objects displaced to a different location. Our results show that animals injected with vehicle preferentially explored the moved object, whereas animals injected with the inverse agonist did not show such preference (Fig. 7, E and F). Total distance travelled by the animals in both memory tests was not significantly affected by injection of GHS-R1a inverse agonist (fig. S3, A and B). Since anxiolytic effects have been observed in mice administered with ghrelin (*12*), we tested performance in the elevated plus maze after blocking ligand-independent activity of GHS-R1a. Consistent with prior results using KO mice for GHS-R1a (*12*), blockade of the ligand-independent activity of GHS-R1a did not affect performance in the elevated plus maze (Fig. 7G, and fig. S3, C and D).The total distance travelled by animals in this test was also not affected by injections (fig. S3 E). Our results indicate that acute blockade of the ligand-independent GHS-R1a activity impairs performance during the novel object recognition task and in the object displacement recognition task, which suggests that tonic activity of GHS-R1a is important for learning and memory.

Discussion

The ligand-independent activity of GHS-R1a has been previously described to regulate food intake and body weight (*18, 20*). Here, we provide strong evidence for the presence of ligand-independent activity of GHS-R1a in the hippocampus, and that it regulates AMPARs levels at the synapse and the formation of spatial memories. ~~We~~ Overall, our results show a dual role for the ligand-independent GHS-R1a activity: on one hand, it promotes the synaptic accumulation of AMPARs, thereby regulating synaptic

transmission; on the other hand, by regulating the availability of cell surface GHS-R1a, it limits the capacity of the hormone ghrelin to modulate AMPARs at the synapse through the activation of GHS-R1a. We further found that blocking the ligand-independent GHS-R1a activity enhances the mobility of synaptic AMPARs, decreasing AMPAR residence at synapses, and impairs synaptic plasticity in the hippocampus. Our data indicate that this control is produced through the phosphorylation of GluA1 Ser^{845} by PKA, which has been shown to regulate extrasynaptic membrane trafficking of GluA1, and to prime AMPARs for synaptic insertion upon the induction of synaptic plasticity (*46*). Interestingly, phosphorylation of this site is also required for retention of spatial learning (*53*).

We found that in organotypic hippocampal slices blockade of the ligand-independent activity of GHS-R1a led to decreased phosphorylation in CaMKIV and GluA1 Ser^{845}, but not to changes in the PKC phosphorylation site in GluA1 (Ser^{831}), despite increased PIP$_2$ levels in hippocampal neurons incubated with the GHS-R1 inverse agonists. Ligand-independent activity of GHS-R1a has been demonstrated both by measuring IP$_3$ turnover and by using assays for transcription activity controlled by cAMP-responsive element (CRE) (*21, 43*). Blockade of basal signaling from GHS-R1a in cultured mouse hypothalamic cells using SP-A led to decreased CRE-binding protein (CREB) phosphorylation (*20*), but signaling downstream of the ligand-independent activity of GHS-R1a in the hippocampus has not been explored before. Our data now suggest that the ligand-independent activity of GHS-R1a may impact G$_q$/PLC/IP$_3$-, CaMKIV- and PKA-dependent pathways, and lead to changes in phosphorylation levels of GluA1 in the hippocampus,

In order to assess the physiological relevance of the ligand-independent activity of GHS-R1a we tested the effect of its blockade on the memory for object novelty and location. We observed that blocking the ligand-independent activity of GHS-R1a impairs recognition and spatial memory. This effect is in agreement with the observation that GHS-R1a KO mice perform poorly in memory tests (*36, 37*), and suggests a clear role in

memory for the unusually high ligand-independent activity of GHS-R1a, an intrinsic feature of this receptor (*54*).

Besides signaling in response to ghrelin, and in the absence of the ligand, GHS-R1a has recently been shown to modulate dopamine signaling through heterodimerization with dopamine receptors DRD1 and DRD2 (*55, 56*). In the hippocampus, GHS-R1a and DRD1 form heteromers that are activated by DRD1 agonists to induce intracellular Ca^{2+} mobilization, activation of early synaptic plasticity markers, and to modulate memory (*56*). Importantly, the dopamine-induced effect on Ca^{2+} signaling is independent of the ligand-independent activity of GHS-R1a in the GHS-R1a:DRD1 complex (*56*). This suggests that the role of the ligand-independent activity of GHS-R1a on memory here described runs parallel to the effects of dopamine on memory through the GHS-R1a:DRD1 complex.

The ligand-independent GHS-R1a activity has also been shown to reduce presynaptic Ca_v2 currents and GABA release in hypothalamic and hippocampal neurons (*57, 58*), by reducing the cell surface expression of Ca_v2 channels (*59*). Our results complement this observation, but further work should be done to explore how the effects of the ligand-independent activity of GHS-R1a on the inhibitory and excitatory systems contribute to memory formation.

It was recently reported that the melanocortin receptor accessory protein 2 (MRAP2) controls GHS-R1a signaling by inhibiting its ligand-independent activity, as well as by increasing its G protein-mediated signaling and blocking the recruitment and signaling of β-arrestin elicited by ghrelin binding (*60*). Disruption of the gene for *MRAP2* has been associated with obesity in animal models and humans (*61*). *MRAP2* mRNA has low expression in the hippocampus of both animals (*61, 62*) and humans (*63*), which suggests that ligand-independent activity of GHS-R1a is unimpeded in this region and is thus more likely to have an influence in hippocampal excitatory synapse protein dynamics and hippocampal-dependent behavior. In fact we observed PIP_2 membrane

accumulation in hippocampal neurons treated with GHS-R1a inverse agonists, in direct support of basal ligand-independent activity of GHS-R1a in hippocampal neurons.

Recent evidence suggests that the ligand-independent activity of the receptor is endogenously regulated by the plasmatic levels of LEAP2 (*34*), which are proportional to the levels of adiposity and blood glucose (*33*). The levels of ligand-independent activity of GHS-R1are highly dependent on the expression levels of the receptor (*20*), which in turn change according to the animal´s feeding status (*19, 20*). Therefore, our observations support a physiological mechanism in which the internal metabolic state of animals exerts control over cognitive processes. The ligand-independent activity of GHS-R1a may be particularly important in the hippocampus, given that, in contrast to the hypothalamus—which is in close proximity to fenestrated capillaries, access of plasma ghrelin to the hippocampal structure may be more limited [reviewed in (*64*)], and it is still a matter of debate whether ghrelin can be produced in the brain (*65*).

Certainly, the role of the ligand-independent GHS-R1a activity reported in this work should be taken into account when considering GHS-R1a inverse agonists as treatments for obesity (*66*) or alcohol use disorders (*38, 39*).

Materials and Methods

Materials

The GHS-R1a inverse agonist [D-Arg[1],D-Phe[5],D-Trp[7,9],Leu[11]]-substance P (SP-A) was purchased from Bachem (Bubendorf, Switzerland), the AZ12861903 (AZ) GHS-R1a inverse agonist was kindly provided by AstraZeneca. The GHS-R1a agonist MK-0677 was purchased from Axon Medchem (Groningen, The Netherlands). The GHS-R1a antagonist [D-Lys[3]]-GHRP-6, TTX, and picrotoxin were purchased from Tocris Bioscience (Bristol, UK), the GHS-R1a antagonist JMV 2959 was obtained from Calbiochem (Merck Millipore, Portugal). The anti-Tubulin antibody was purchased from Sigma-Aldrich (Sintra, Portugal); the anti-Akt, anti-P-Ser[473](Akt), anti-PSD95 (rabbit), and anti-CaMKIV antibodies were obtained from Cell Signaling (Danvers, MA, USA); the anti-GluA1, anti-GluA2, anti-P-Ser[845](GluA1), anti-P-Ser[239/240] (Stargazin) and anti-VGluT1 antibodies were from Millipore (Madrid, Spain); the anti-MAP2 antibody was from Abcam (Cambridge, UK), the anti-P-Ser[831](GluA1) antibody was from Tocris Bioscience (Bristol,UK), the anti-PSD95 (mouse) antibody was from Affinity BioReagents (Golden, USA), and the anti-P-Thr[196] (CaMKIV) antibody was from Santa Cruz Biotechnology Inc (Santa Cruz, CA); the anti-GFP (rabbit) antibody was from MBL International (Woburn, USA) and the anti-GFP (mouse) antibody was from Roche (Amadora, Portugal). Quantum dots (QDs) 655 Goat F(ab')2 anti-mouse IgG conjugate (H^{+}L) were purchased from Invitrogen (Barcelona, Spain). The antibody for the N-terminus of GluA1 was a kind gift from Dr. Andrew Irving (University College Dublin). All other reagents were purchased from Sigma-Aldrich (Sintra, Portugal), Fisher Chemicals or from Merck (Darmstadt, Germany) unless specified otherwise.

DNA constructs

For the generation of the short hairpin interfering RNA construct targeting GHS-R1a, a previously described and validated sequence (*42*) was used. Complementary

oligonucleotides, each containing a unique 19-nt sequence derived from within the target mRNA transcripts of *ghsr1a* gene (NM_032075) targeting nucleotides 79-96 (GACTCACTGCCTGACGAAC) (*42*), were annealed and subcloned into the HpaI/XhoI sites of the U6 promoter-driven short hairpin RNA expression vector pLentiLox3.7(CMV)EGFP, which co-expresses EGFP under the CMV promoter. The control shRNA that targets firefly luciferase was described previously (*67*). Homer1C-DsRed and Homer1C-GFP were previously described (*68*). PLCδPH-GFP was a gift from Tamas Balla (Addgene plasmid #51407) (*41*).

Neuronal and slice cultures

Primary cultures of rat hippocampal neurons were prepared as previously described (*69*). Hippocampal slices were prepared from young Wistar rats of either sex (postnatal day 5–6) as previously described (*70*).

Neuron transfection

DNA constructs expressing [Luciferase shRNA-GFP, GHS-R1a shRNA-GFP (Knock-down), hGHS-R1a (rescue), SEP-GluA1, Homer1C-DsRed and Homer1C-GFP] or [PLCδPH-GFP and mCherry] were expressed in primary cultures of hippocampal neurons either at 9 DIV or 13-14 DIV, respectively, using an adapted calcium phosphate transfection protocol (*71*), as previously described (*69*).

Application of GHS-R1a inverse agonists, antagonists and agonist

Hippocampal organotypic slices (6 DIV) were treated with the GHS-R1a inverse agonist [D-Arg^1, D-Phe^5,D-Trp^{7,9},Leu^{11}]-substance P (SP-A, 1µM) for 20 h, or chronically treated with the GHS-R1a antagonist [D-Lys^3]-GHRP-6 (100 µM) from 3 DIV up to 7 DIV. Hippocampal neurons in culture were incubated with the GHS-R1a inverse agonists SP-A and AZ1286190 (AZ, 50 nM), antagonist JMV2959 (100 µM) and agonist MK-0677 (1 µM). The compounds were added directly to the culture medium. AZ for injection in vivo

was dissolved in 95% beta-hydroxypropylcyclodextrin (**β**-hpC)/5% v/v DMSO. **β**-hpC was prepared at 25 % w/v in Sorenson's buffer pH 5.5. All the injected solutions were prepared in sterile conditions. The drug and vehicle were injected intraperitoneally at volumes of 100-150 µl. The dose of 100 mg/kg was based on previously described doses by McCoull and colleagues (*25*).

Imaging and analysis of PLCδPH-GFP translocation

For live-cell imaging experiments, hippocampal neurons (15-16 DIV) transfected with the PLCδPH-GFP construct were imaged with a spinning-disk confocal microscope using a LCI Plan-Neofluar 63×/1.3 objective. Cultured hippocampal neurons were kept at 37ºC and perfused with Sham medium (10 mM HEPES, 0,116 M NaCl, 5,4 mM KCl, 0,8 mM MgSO$_4$, 1 mM NaH$_2$PO$_4$, 25 mM glucose, 1,8 mM CaCl$_2$ 25 mM NaHCO$_3$,, pH 7,3) while imaging. To analyse PLCδPH-GFP translocation, regions of interest (ROI) were defined in the cytosol or membrane regions of dendrites. The fluorescence intensity inside ROIs (F) was normalized to baseline values (F$_0$), before the application of MK-0677 or SP-A. Three ROIs (each for cytoplasm and membrane regions) were analysed and averaged per neuron. All fluorescence measurements were performed using ImageJ software. Images obtained from experiments in fixed cells were captured on a Leica SP8 laser-scanning confocal microscope. To quantify the spine/shaft ratio of PLCδPH-GFP fluorescence intensity in fixed neurons, line profiles were traced along the dendritic spine heads, the plasma membrane of the dendritic shaft and the cytosol of the dendritic shaft, and the mean fluorescence intensity of PLCδPH-GFP from the spine and respective dendritic shaft was determined by using the plot profile tool from ImageJ software. An average of 5-10 spine/shaft ratios were used per neuron.

Immunocytochemistry

For labeling surface GluA1-containing AMPARs, live neurons were incubated for 10 min at room temperature using an antibody against an extracellular epitope in the GluA1 N-terminus diluted in conditioned neuronal culture medium or extracellular solution (used

for chemical LTP). Neurons were then fixed and stained as previously described (*69*).

For labeling GluA2-containing AMPARs, neurons were fixed and then incubated overnight with an anti-GluA2 antibody diluted 1:100 in 3%BSA/PBS, at 4°C. Neurons were then stained as previously described (*69*).

Quantitative imaging analysis

Imaging was performed on a Zeiss Axio Observer Z1 microscope using a Plan Apochromat 63×/1.4 NA oil objective, and an AxioCam HRm CCD camera. Images were quantified using image analysis software ImageJ. For quantification of total fluorescence intensity of GluA1 cell-surface puncta and GluA1 synaptic clusters (VGluT1/PSD95-colocalized or VGluT1-colocalized) sets of cells were cultured and stained simultaneously and imaged using identical settings. The region of interest was randomly selected avoiding primary dendrites, and dendritic length was measured using MAP2 staining. Measurements were performed in 2 to 5 independent preparations, and at least 7 cells per condition were analyzed for each preparation. Quantitative imaging analysis was performed as previously described (*69*).

Electrophysiology

Voltage-clamp whole-cell recordings were performed stimulating Schaffer collateral fibers and recording evoked synaptic responses from CA1 pyramidal neurons at different holding potentials. The AMPA/NMDA ratios were calculated by acquiring AMPARs responses at –60 mV and NMDA receptors responses at +40 mV at a latency at which AMPARs responses were fully decayed (60 ms after stimulation). Picrotoxin (100 μM) was present in the external solution to block the $GABA_A$ receptor responses. The recording chamber was perfused with external solution (in mM: 119 NaCl, 2.5 KCl, 1 NaH_2PO_4, 11 glucose, 26 $NaHCO_3$, 4 $MgCl_2$, 4 $CaCl_2$ and 0.004 2-chloroadenosine, at pH 7.4), and was gassed with 5% CO_2/ 95% O_2. Patch recording pipettes (3–6 M Ω) were filled with internal solution (in mM: 115 $CsMeSO_3$, 20 CsCl, 10 HEPES, 2.5 MgCl2, 4

Na$_2$ATP, 0.4 Na$_3$GTP, 10 sodium phosphocreatine and 0.6 EGTA, at pH 7.25). Synaptic responses were evoked with bipolar electrodes using single-voltage pulses (200 µs, up to 20 V). The stimulating electrodes were placed over Schaffer collateral fibers between 300 and 500 µm from the CA1 recorded cells. Synaptic responses were averaged over 50 trials. Whole-cell recordings were carried out with a Multiclamp 700A amplifier (Molecular Devices, Sunnyvale, USA).

chemical LTP (cLTP) protocol

cLTP was induced as previously described (*45*). 19 DIV hippocampal cultures were washed with extracellular solution (ECS) containing (in mM): 150 NaCl, 2 CaCl$_2$, 5 KCl, 10 HEPES, 30 Glucose, 0.001 TTX, 0.01 strychnine, 0.03 picrotoxin, pH 7.4. After washing, neurons were stimulated with glycine (300 µM) at room temperature for 3 min in ECS and then incubated for 20–25 min in ECS in a 37°C, 5% CO$_2$/95% air incubator.

Quantum dots labeling and Imaging

Endogenous GluA2 and GluA1-SEP labeling was performed in two steps: first neurons were incubated for 10 min at 37°C with anti-GFP antibody (1/300000) or anti-GluA2 antibody (1/1000), diluted in conditioned medium. After one washing step, anti-mouse IgG conjugated QD655 (diluted 1:10 in PBS) were diluted in conditioned medium with BSA 2% (1/2000) and were incubated on cells for 5 min at 37°C. Synapses were labeled using transfection with Homer1C-DsRed or Homer1C-GFP. All washes were performed in ECS containing (in mM) NaCl 145, KCl 5, Glucose 10, Hepes 10, CaCl$_2$ 2 and MgCl$_2$ 2), supplemented with BSA 2% at 37°C. After washing, neurons were mounted in an open chamber (K.F. Technology SRL) and imaged in ECS. Single particle tracking was performed as in (*72*). Cells were imaged at 37°C on an inverted microscope (AxioObserver Z1, Carl Zeiss) equipped with a Plan Apochromat 63× oil objective (NA = 1.4). QDs, Homer1C-DsRed and Homer1C-GFP signals were detected by using a HXP fluorescence lamp (For QDs: excitation filter 425/50 and emission filters 655/30,

Chroma). Fluorescent images from QDs were obtained with an integration time of 50 ms with up to 600 consecutive frames. Signals were recorded with a digital CMOS camera (ORCA Flash 4.0, Hamamatsu). QD-labeled GluAs were imaged on randomly selected dendritic regions over up to 30 min total experimental time. QDs fixed on the coverslip allowed us to compensate mechanical drifts of the stage.

Quantum dots Tracking and Analysis

The tracking of single QDs was performed with homemade software based on Matlab (Mathworks Inc., Natick, USA). Single QDs were identified by their diffraction limited signals and their blinking fluorescent emission. The trajectory of a QD tagged receptor could not be tracked continuously due to the random blinking events of the QDs. When the positions before and after the dark period were compatible with borders set for maximal position changes between consecutive frames and blinking rates, the subtrajectories of the same receptor were reconnected. The values were determined empirically: 2–3 pixels (0.32–0.48 µm) for maximal position change between two frames and maximal dark periods of 25 frames (1.25 s). MSD curves were calculated for reconnected trajectories of at least 20 frames. The QDs were considered synaptic if colocalized with Homer dendritic clusters for at least five frames. Diffusion coefficients were calculated by a linear fit of the first 4–8 points of the mean square displacement (MSD) plots versus time depending on the length of the trajectory within a certain compartment. The resolution limit for diffusion was 0.0075 μm^2/s as determined by (*73*), whereas the resolution precision was ~40 nm.

Biochemistry

Protein extracts were prepared in lysis buffer [10 mM HEPES (pH 7.4), 150 mM NaCl, 10 mM EDTA, 1% (v/v) Triton X-100 supplemented with 1 mM DTT, 0.1 mM phenylmethylsulfonyl (PMSF), 1 µg/ml chymostatin, 1 µg/ml leupeptin, 1 µg/ml antipain, 1 µg/ml pepstatin (CLAP) and a cocktail of phosphatase inhibitors (1x, Roche, Carnaxide,

Portugal)]. After centrifugation at 16,100 x g for 10 min at 4°C, protein in the supernatant was quantified using the bicinchoninic acid (BCA) assay kit (Pierce, Termo Fisher Scientific, Rockford, USA), and the samples were denatured with 5x concentrated denaturating buffer [62.5 mM Tris-HCl (pH 6.8), 10% (v/v) Glicerol, 2% (v/v) SDS, 0.01% (w/v) bromophenol blue and 5% (v/v) β-mercaptoethanol (added fresh)], and boiled for 5 min. Protein extracts were resolved by SDS-PAGE in 7.5% or 12% polyacrylamide gels. For western blot analysis, proteins were transferred onto a PVDF membrane (Millipore, Madrid, Spain) by electroblotting (40 V, overnight at 4°C). The membranes were blocked for 1 h at room temperature in Tris-buffered saline (137 mM NaCl, 20 mM Tris-HCl, pH 7.6) containing 0.1% (v/v) Tween-20 (TBS-T), and 5% (w/v) low-fat milk or BSA. Membranes were probed during 1 h, at room temperature, or overnight, at 4°C, with the primary antibodies diluted in TBS-T containing 5% or 0.5% (w/v) low-fat milk or 5% (w/v) BSA. Following several washes, membranes were incubated for 1 h with alkaline phosphatase-conjugated secondary antibodies (anti-mouse or anti- rabbit, depending on the primary antibody host species) at room temperature, washed again and incubated with chemifluorescent substrate (ECF) (GE Heathcare, Carnaxide, Portugal) for 5 min at room temperature. Membranes were scanned with the Storm 860 scanner (GE Heathcare, Carnaxide, Portugal), and quantified using the ImageQuant software under linear exposure conditions. When necessary, the membranes were stripped (0.2 M NaOH for 5 min) and re-probed.

Animals and Behavior

For the behavior experiments, 8- to 15-week-old male C56BL/6 mice were housed in the Animal Facility of the CNC/Faculty of Medicine of the University of Coimbra with access to food and water *ad libitum.* The environment was kept in controlled temperature and humidity conditions under a 12-hour dark-light cycle (light period 6h00-18h00). Behavioral testing was reviewed and approved by the animal use and ethics committee (ORBEA) of the CNC/Faculty of Medicine, University of Coimbra, and by the Portuguese

national authority for animal experimentation (DGAV), and all procedures were performed according to the guidelines of the DGAV and Directive 2010/63/EU of the European Parliament.

The novel object recognition task was adapted from Leger and colleagues (*48*). This task consisted of 3 phases: In a first phase the animals freely explored the empty open-field arena for 10 min (habituation phase). Twenty four hours after, the animals were allowed to explore two similar, symmetrically disposed objects, for 10 min. Ten minutes before this phase the animals were submitted to intraperitoneal injection of either the drug or the vehicle, and stayed in an empty transport cage before entering the training phase. Six hours after the training phase, the animals were exposed to 2 objects located in the same positions as previously, but this time one of the objects was substituted by a new object that the animal had not contacted previously (test phase).

The object displacement test was adapted from Oliveira and colleagues (*49*). The test took place during 2 days. During the first day the animals were allowed to explore an empty open-field for 6 min (habituation phase). Immediately after, the animals were intraperitoneally injected with the inverse agonist of GHS-R1a or its respective vehicle and placed in their homecage. After 10 minutes, the animals explored two different objects placed in a specific location of the open field for 6 minutes (training phase). The animals were then returned to their homecage and waited for 3 minutes. Two more similar training phases were conducted, with a 3 minute waiting period in between. On the next day, the animals returned to the open field, where one of the objects was placed in a new location, and were allowed to explore the objects for 6 minutes (test phase).

The objects and their positions were randomized for both tests. The used objects correspond those the described by Leger and colleagues (*48*). The arena and the objects were carefully cleaned before running each animal and in between phases. The test was conducted at a room temperature of 23°C and 15 lux at the center of the arena (homogenously distributed light). Videos of the test were acquired using Noldus

Ethovision software and scoring was performed blinded to treatment of the animals, using Noldus Observer.

The elevated plus maze was performed according to (*74*), using a maze made in-house according to previously described specifications (*75*). Animals were weighted and injected with the corresponding dose of inverse agonist or vehicle 10 min before starting the test, and stayed in an empty transport cage. The test started by putting the animals in the central part of the maze with the nose aligned with the closed arms, and run for 10 min. The test was conducted under 100 lux at the center of the arena. The arena was carefully cleaned before and after each run. Videos of the test were acquired and automatically quantified using Noldus Ethovision.

Statistical analysis

We first evaluated the adjustment of quantitative sample distributions to a theoretical normal one using the Shapiro-Wilk test. Even when quantitative sample distributions were considered to fit a gaussian, if more than two non-balanced groups were in analysis the Bartlett's test for homoscedasticity was considered to decide whenever to apply parametric or nonparametric tests. Mann-Whitney test, unpaired *t*-test or paired *t*-test were used to compare statistical differences between any two groups. Comparisons between multiple groups were performed with the Kruskal-Wallis analysis of variance followed by Dunn's multiple comparison test or with one-way ANOVA followed by Dunnett's multiple comparison test. In addition, data of behavioral tests were analyzed using Wilcoxon matched-pairs signed rank test or two-way ANOVA with Bonferroni adjustment for correction of multiple comparisons. Data was analyzed using Graphpad Prism 7.04 and results were evaluated at a 5% significance level.

Figure S1. **Blockage of the ligand-independent activity of GHS-R1a decreases the synapse density in mature primary cultured hippocampal neurons.**

Figure S2. **Blockage of the ligand-independent activity of GHS-R1a increases the cell surface diffusion of GluA2-AMPARs.**

Figure S3. **Administration of an inverse agonist of GHS-R1a does not impair overall movement.**

Movie S1. **Application of the GHS-R1a agonist MK-0677 induces the translocation of PLCδPH-GFP from the plasma membrane into the cytosol.**

Movie S2. **Application of the GHS-R1a inverse agonist SP-A increases the plasma membrane levels of PLCδPH-GFP.**

References and Notes:

1. M. Kojima, H. Hosoda, Y. Date, M. Nakazato, H. Matsuo, K. Kangawa, Ghrelin is a growth-hormone-releasing acylated peptide from stomach. *Nature* **402**, 656-660 (1999); published online EpubDec 9 (10.1038/45230).

2. M. Nakazato, N. Murakami, Y. Date, M. Kojima, H. Matsuo, K. Kangawa, S. Matsukura, A role for ghrelin in the central regulation of feeding. *Nature* **409**, 194-198 (2001); published online EpubJan 11 (10.1038/35051587).

3. D. E. Cummings, J. Q. Purnell, R. S. Frayo, K. Schmidova, B. E. Wisse, D. S. Weigle, A preprandial rise in plasma ghrelin levels suggests a role in meal initiation in humans. *Diabetes* **50**, 1714-1719 (2001); published online EpubAug (

4. Y. Date, M. Kojima, H. Hosoda, A. Sawaguchi, M. S. Mondal, T. Suganuma, S. Matsukura, K. Kangawa, M. Nakazato, Ghrelin, a novel growth hormone-releasing acylated peptide, is synthesized in a distinct endocrine cell type in the gastrointestinal tracts of rats and humans. *Endocrinology* **141**, 4255-4261 (2000); published online EpubNov (10.1210/endo.141.11.7757).

5. B. L. Mason, Q. Wang, J. M. Zigman, The central nervous system sites mediating the orexigenic actions of ghrelin. *Annu Rev Physiol* **76**, 519-533 (2014)10.1146/annurev-physiol-021113-170310).

6. T. M. Hsu, J. D. Hahn, V. R. Konanur, E. E. Noble, A. N. Suarez, J. Thai, E. M. Nakamoto, S. E. Kanoski, Hippocampus ghrelin signaling mediates appetite through lateral hypothalamic orexin pathways. *eLife* **4**, (2015); published online EpubDec 15 (10.7554/eLife.11190).

7. S. E. Kanoski, S. M. Fortin, K. M. Ricks, H. J. Grill, Ghrelin signaling in the ventral hippocampus stimulates learned and motivational aspects of feeding via PI3K-Akt signaling. *Biological psychiatry* **73**, 915-923 (2013); published online EpubMay 1 (10.1016/j.biopsych.2012.07.002).

8. D. Serrenho, S. D. Santos, A. L. Carvalho, The Role of Ghrelin in Regulating Synaptic Function and Plasticity of Feeding-Associated Circuits. *Front Cell Neurosci* **13**, 205 (2019)10.3389/fncel.2019.00205).

9. V. P. Carlini, M. E. Monzon, M. M. Varas, A. B. Cragnolini, H. B. Schioth, T. N. Scimonelli, S. R. de Barioglio, Ghrelin increases anxiety-like behavior and memory retention in rats. *Biochem Biophys Res Commun* **299**, 739-743 (2002); published online EpubDec 20 (S0006291X02027407 [pii]).

10. S. Diano, S. A. Farr, S. C. Benoit, E. C. McNay, I. da Silva, B. Horvath, F. S. Gaskin, N. Nonaka, L. B. Jaeger, W. A. Banks, J. E. Morley, S. Pinto, R. S. Sherwin, L. Xu, K. A. Yamada, M. W. Sleeman, M. H. Tschop, T. L. Horvath, Ghrelin controls hippocampal spine synapse density and memory performance. *Nat Neurosci* **9**, 381-388 (2006); published online EpubMar (nn1656 [pii]

10.1038/nn1656).

11. A. Abizaid, Z. W. Liu, Z. B. Andrews, M. Shanabrough, E. Borok, J. D. Elsworth, R. H. Roth, M. W. Sleeman, M. R. Picciotto, M. H. Tschop, X. B. Gao, T. L. Horvath, Ghrelin modulates the activity and synaptic input organization of midbrain dopamine neurons while promoting appetite. *J Clin Invest* **116**, 3229-3239 (2006); published online EpubDec (10.1172/JCI29867).

12. M. Lutter, I. Sakata, S. Osborne-Lawrence, S. A. Rovinsky, J. G. Anderson, S. Jung, S. Birnbaum, M. Yanagisawa, J. K. Elmquist, E. J. Nestler, J. M. Zigman, The orexigenic hormone ghrelin defends against depressive symptoms of chronic stress. *Nat Neurosci* **11**, 752-753 (2008); published online EpubJul (nn.2139 [pii]

10.1038/nn.2139).

13.   R. M. Meyer, A. Burgos-Robles, E. Liu, S. S. Correia, K. A. Goosens, A ghrelin-growth hormone axis drives stress-induced vulnerability to enhanced fear. *Molecular psychiatry* **19**, 1284-1294 (2014); published online EpubDec (10.1038/mp.2013.135).

14.   M. A. Cowley, R. G. Smith, S. Diano, M. Tschop, N. Pronchuk, K. L. Grove, C. J. Strasburger, M. Bidlingmaier, M. Esterman, M. L. Heiman, L. M. Garcia-Segura, E. A. Nillni, P. Mendez, M. J. Low, P. Sotonyi, J. M. Friedman, H. Liu, S. Pinto, W. F. Colmers, R. D. Cone, T. L. Horvath, The distribution and mechanism of action of ghrelin in the CNS demonstrates a novel hypothalamic circuit regulating energy homeostasis. *Neuron* **37**, 649-661 (2003); published online EpubFeb 20 (S0896627303000631 [pii]).

15.   L. F. Ribeiro, T. Catarino, S. D. Santos, M. Benoist, J. F. van Leeuwen, J. A. Esteban, A. L. Carvalho, Ghrelin triggers the synaptic incorporation of AMPA receptors in the hippocampus. *Proc Natl Acad Sci U S A* **111**, E149-158 (2014); published online EpubJan 7 (10.1073/pnas.1313798111).

16.   L. Shi, X. Bian, Z. Qu, Z. Ma, Y. Zhou, K. Wang, H. Jiang, J. Xie, Peptide hormone ghrelin enhances neuronal excitability by inhibition of Kv7/KCNQ channels. *Nature communications* **4**, 1435 (2013)10.1038/ncomms2439).

17.   X. M. Guan, H. Yu, O. C. Palyha, K. K. McKee, S. D. Feighner, D. J. Sirinathsinghji, R. G. Smith, L. H. Van der Ploeg, A. D. Howard, Distribution of mRNA encoding the growth hormone secretagogue receptor in brain and peripheral tissues. *Brain Res Mol Brain Res* **48**, 23-29 (1997); published online EpubAug (S0169328X97000715 [pii]).

18.   G. Fernandez, A. Cabral, M. F. Andreoli, A. Labarthe, C. M'Kadmi, J. G. Ramos, J. Marie, J. A. Fehrentz, J. Epelbaum, V. Tolle, M. Perello, Evidence Supporting a Role for Constitutive Ghrelin Receptor Signaling in Fasting-Induced Hyperphagia in Male Mice. *Endocrinology* **159**, 1021-1034 (2018); published online EpubFeb 1 (10.1210/en.2017-03101).

19.   M. S. Kim, C. Y. Yoon, K. H. Park, C. S. Shin, K. S. Park, S. Y. Kim, B. Y. Cho, H. K. Lee, Changes in ghrelin and ghrelin receptor expression according to feeding status. *Neuroreport* **14**, 1317-1320 (2003); published online EpubJul 18 (10.1097/01.wnr.0000078703.79393.d2).

20.   P. S. Petersen, D. P. Woldbye, A. N. Madsen, K. L. Egerod, C. Jin, M. Lang, M. Rasmussen, A. G. Beck-Sickinger, B. Holst, In vivo characterization of high basal signaling from the ghrelin receptor. *Endocrinology* **150**, 4920-4930 (2009); published online EpubNov (10.1210/en.2008-1638).

21.   B. Holst, A. Cygankiewicz, T. H. Jensen, M. Ankersen, T. W. Schwartz, High constitutive signaling of the ghrelin receptor--identification of a potent inverse agonist. *Molecular endocrinology* **17**, 2201-2210 (2003); published online EpubNov (10.1210/me.2003-0069).

22.   M. Damian, S. Mary, M. Maingot, C. M'Kadmi, D. Gagne, J. P. Leyris, S. Denoyelle, G. Gaibelet, L. Gavara, M. Garcia de Souza Costa, D. Perahia, E. Trinquet, B. Mouillac, S. Galandrin, C. Gales, J. A. Fehrentz, N. Floquet, J. Martinez, J. Marie, J. L. Baneres, Ghrelin receptor conformational dynamics regulate the transition from a preassembled to an active receptor:Gq complex. *Proc Natl Acad Sci U S A* **112**, 1601-1606 (2015); published online EpubFeb 3 (10.1073/pnas.1414618112).

23.   M. P. Cornejo, D. Castrogiovanni, H. B. Schioth, M. Reynaldo, J. Marie, J. A. Fehrentz, M. Perello, Growth hormone secretagogue receptor signalling affects high-fat intake independently of plasma levels of ghrelin and LEAP2, in a 4-day binge eating model. *Journal of neuroendocrinology* **31**, e12785 (2019); published online EpubOct (10.1111/jne.12785).

24.   S. Els, E. Schild, P. S. Petersen, T. M. Kilian, J. Mokrosinski, T. M. Frimurer, C. Chollet, T. W. Schwartz, B. Holst, A. G. Beck-Sickinger, An aromatic region to induce a switch

between agonism and inverse agonism at the ghrelin receptor. *J Med Chem* **55**, 7437-7449 (2012); published online EpubSep 13 (10.1021/jm300414b).

25. W. McCoull, P. Barton, A. J. Brown, S. S. Bowker, J. Cameron, D. S. Clarke, R. D. Davies, A. G. Dossetter, A. Ertan, M. Fenwick, C. Green, J. L. Holmes, N. Martin, D. Masters, J. E. Moore, N. J. Newcombe, C. Newton, H. Pointon, G. R. Robb, C. Sheldon, S. Stokes, D. Morgan, Identification, optimization, and pharmacology of acylurea GHS-R1a inverse agonists. *J Med Chem* **57**, 6128-6140 (2014); published online EpubJul 24 (10.1021/jm500610n).

26. N. Li, G. Song, Y. Wang, Q. Zhu, F. Han, C. Zhang, Y. Zhou, Blocking constitutive activity of GHSR1a in the lateral amygdala facilitates acquisition of conditioned taste aversion. *Neuropeptides* **68**, 22-27 (2018); published online EpubApr (10.1016/j.npep.2017.12.001).

27. H. Inoue, N. Kangawa, A. Kinouchi, Y. Sakamoto, C. Kimura, R. Horikawa, Y. Shigematsu, M. Itakura, T. Ogata, K. Fujieda, C. Japan Growth Genome, Identification and functional analysis of novel human growth hormone secretagogue receptor (GHSR) gene mutations in Japanese subjects with short stature. *The Journal of clinical endocrinology and metabolism* **96**, E373-378 (2011); published online EpubFeb (10.1210/jc.2010-1570).

28. J. Pantel, M. Legendre, S. Cabrol, L. Hilal, Y. Hajaji, S. Morisset, S. Nivot, M. P. Vie-Luton, D. Grouselle, M. de Kerdanet, A. Kadiri, J. Epelbaum, Y. Le Bouc, S. Amselem, Loss of constitutive activity of the growth hormone secretagogue receptor in familial short stature. *J Clin Invest* **116**, 760-768 (2006); published online EpubMar (10.1172/JCI25303).

29. J. Pantel, M. Legendre, S. Nivot, S. Morisset, M. P. Vie-Luton, Y. le Bouc, J. Epelbaum, S. Amselem, Recessive isolated growth hormone deficiency and mutations in the ghrelin receptor. *The Journal of clinical endocrinology and metabolism* **94**, 4334-4341 (2009); published online EpubNov (10.1210/jc.2009-1327).

30. H. J. Wang, F. Geller, A. Dempfle, N. Schauble, S. Friedel, P. Lichtner, F. Fontenla-Horro, S. Wudy, S. Hagemann, L. Gortner, K. Huse, H. Remschmidt, T. Bettecken, T. Meitinger, H. Schafer, J. Hebebrand, A. Hinney, Ghrelin receptor gene: identification of several sequence variants in extremely obese children and adolescents, healthy normal-weight and underweight students, and children with short normal stature. *The Journal of clinical endocrinology and metabolism* **89**, 157-162 (2004); published online EpubJan (10.1210/jc.2003-031395).

31. L. J. Torz, S. Osborne-Lawrence, J. Rodriguez, Z. He, M. P. Cornejo, E. R. Mustafa, C. Jin, N. Petersen, M. A. Hedegaard, M. Nybo, V. M. Damonte, N. P. Metzger, B. K. Mani, K. W. Williams, J. Raingo, M. Perello, B. Holst, J. M. Zigman, Metabolic insights from a GHSR-A203E mutant mouse model. *Molecular metabolism* **39**, 101004 (2020); published online EpubSep (10.1016/j.molmet.2020.101004).

32. X. Ge, H. Yang, M. A. Bednarek, H. Galon-Tilleman, P. Chen, M. Chen, J. S. Lichtman, Y. Wang, O. Dalmas, Y. Yin, H. Tian, L. Jermutus, J. Grimsby, C. M. Rondinone, A. Konkar, D. D. Kaplan, LEAP2 Is an Endogenous Antagonist of the Ghrelin Receptor. *Cell Metab* **27**, 461-469 e466 (2018); published online EpubFeb 6 (10.1016/j.cmet.2017.10.016).

33. B. K. Mani, N. Puzziferri, Z. He, J. A. Rodriguez, S. Osborne-Lawrence, N. P. Metzger, N. Chhina, B. Gaylinn, M. O. Thorner, E. L. Thomas, J. D. Bell, K. W. Williams, A. P. Goldstone, J. M. Zigman, LEAP2 changes with body mass and food intake in humans and mice. *J Clin Invest* **129**, 3909-3923 (2019); published online EpubSep 3 (10.1172/JCI125332).

34. C. M'Kadmi, A. Cabral, F. Barrile, J. Giribaldi, S. Cantel, M. Damian, S. Mary, S. Denoyelle, S. Dutertre, S. Peraldi-Roux, J. Neasta, C. Oiry, J. L. Baneres, J. Marie, M. Perello, J. A. Fehrentz, N-Terminal Liver-Expressed Antimicrobial Peptide 2 (LEAP2) Region Exhibits Inverse Agonist Activity toward the Ghrelin Receptor. *J Med Chem* **62**, 965-973 (2019); published online EpubJan 24 (10.1021/acs.jmedchem.8b01644).

35. Y. Mear, A. Enjalbert, S. Thirion, GHS-R1a constitutive activity and its physiological relevance. *Front Neurosci* **7**, 87 (2013)10.3389/fnins.2013.00087).

36. R. G. Albarran-Zeckler, A. F. Brantley, R. G. Smith, Growth hormone secretagogue receptor (GHS-R1a) knockout mice exhibit improved spatial memory and deficits in contextual memory. *Behavioural brain research* **232**, 13-19 (2012); published online EpubJun 15 (10.1016/j.bbr.2012.03.012).

37. J. F. Davis, D. L. Choi, D. J. Clegg, S. C. Benoit, Signaling through the ghrelin receptor modulates hippocampal function and meal anticipation in mice. *Physiology & behavior* **103**, 39-43 (2011); published online EpubApr 18 (10.1016/j.physbeh.2010.10.017).

38. M. R. Lee, M. Farokhnia, E. Cobbina, A. Saravanakumar, X. Li, J. T. Battista, L. A. Farinelli, F. Akhlaghi, L. Leggio, Endocrine effects of the novel ghrelin receptor inverse agonist PF-5190457: Results from a placebo-controlled human laboratory alcohol co-administration study in heavy drinkers. *Neuropharmacology*, 107788 (2019); published online EpubSep 23 (10.1016/j.neuropharm.2019.107788).

39. M. R. Lee, J. D. Tapocik, M. Ghareeb, M. L. Schwandt, A. A. Dias, A. N. Le, E. Cobbina, L. A. Farinelli, S. Bouhlal, M. Farokhnia, M. Heilig, F. Akhlaghi, L. Leggio, The novel ghrelin receptor inverse agonist PF-5190457 administered with alcohol: preclinical safety experiments and a phase 1b human laboratory study. *Molecular psychiatry*, (2018); published online EpubMay 4 (10.1038/s41380-018-0064-y).

40. H. H. Kim, K. H. Lee, D. Lee, Y. E. Han, S. H. Lee, J. W. Sohn, W. K. Ho, Costimulation of AMPA and metabotropic glutamate receptors underlies phospholipase C activation by glutamate in hippocampus. *J Neurosci* **35**, 6401-6412 (2015); published online EpubApr 22 (10.1523/JNEUROSCI.4208-14.2015).

41. P. Varnai, T. Balla, Visualization of phosphoinositides that bind pleckstrin homology domains: calcium- and agonist-induced dynamic changes and relationship to myo-[3H]inositol-labeled phosphoinositide pools. *The Journal of cell biology* **143**, 501-510 (1998); published online EpubOct 19 (10.1083/jcb.143.2.501).

42. Y. B. Shrestha, K. Wickwire, S. Giraudo, Effect of reducing hypothalamic ghrelin receptor gene expression on energy balance. *Peptides* **30**, 1336-1341 (2009); published online EpubJul (10.1016/j.peptides.2009.03.013).

43. B. Holst, N. D. Holliday, A. Bach, C. E. Elling, H. M. Cox, T. W. Schwartz, Common structural basis for constitutive activity of the ghrelin receptor family. *J Biol Chem* **279**, 53806-53817 (2004); published online EpubDec 17 (10.1074/jbc.M407676200).

44. N. D. Holliday, B. Holst, E. A. Rodionova, T. W. Schwartz, H. M. Cox, Importance of constitutive activity and arrestin-independent mechanisms for intracellular trafficking of the ghrelin receptor. *Molecular endocrinology* **21**, 3100-3112 (2007); published online EpubDec (10.1210/me.2007-0254).

45. M. Ahmad, J. S. Polepalli, D. Goswami, X. Yang, Y. J. Kaeser-Woo, T. C. Sudhof, R. C. Malenka, Postsynaptic complexin controls AMPA receptor exocytosis during LTP. *Neuron* **73**, 260-267 (2012); published online EpubJan 26 (10.1016/j.neuron.2011.11.020).

46. M. C. Oh, V. A. Derkach, E. S. Guire, T. R. Soderling, Extrasynaptic membrane trafficking regulated by GluR1 serine 845 phosphorylation primes AMPA receptors for long-term potentiation. *J Biol Chem* **281**, 752-758 (2006); published online EpubJan 13 (10.1074/jbc.M509677200).

47. N. J. Broadbent, L. R. Squire, R. E. Clark, Spatial memory, recognition memory, and the hippocampus. *Proc Natl Acad Sci U S A* **101**, 14515-14520 (2004); published online EpubOct 5 (10.1073/pnas.0406344101).

48. M. Leger, A. Quiedeville, V. Bouet, B. Haelewyn, M. Boulouard, P. Schumann-Bard, T. Freret, Object recognition test in mice. *Nature protocols* **8**, 2531-2537 (2013); published online EpubDec (10.1038/nprot.2013.155).

49. A. M. Oliveira, T. J. Hemstedt, H. Bading, Rescue of aging-associated decline in Dnmt3a2 expression restores cognitive abilities. *Nat Neurosci* **15**, 1111-1113 (2012); published online EpubJul 1 (10.1038/nn.3151).

50. R. L. Huganir, R. A. Nicoll, AMPARs and synaptic plasticity: the last 25 years. *Neuron* **80**, 704-717 (2013); published online EpubOct 30 (10.1016/j.neuron.2013.10.025).

51. P. Opazo, D. Choquet, A three-step model for the synaptic recruitment of AMPA receptors. *Mol Cell Neurosci* **46**, 1-8 (2011); published online EpubJan (10.1016/j.mcn.2010.08.014).

52. A. C. Penn, C. L. Zhang, F. Georges, L. Royer, C. Breillat, E. Hosy, J. D. Petersen, Y. Humeau, D. Choquet, Hippocampal LTP and contextual learning require surface diffusion of AMPA receptors. *Nature* **549**, 384-388 (2017); published online EpubSep 21 (10.1038/nature23658).

53. H. K. Lee, K. Takamiya, J. S. Han, H. Man, C. H. Kim, G. Rumbaugh, S. Yu, L. Ding, C. He, R. S. Petralia, R. J. Wenthold, M. Gallagher, R. L. Huganir, Phosphorylation of the AMPA receptor GluR1 subunit is required for synaptic plasticity and retention of spatial memory. *Cell* **112**, 631-643 (2003); published online EpubMar 7 (

54. M. Damian, J. Marie, J. P. Leyris, J. A. Fehrentz, P. Verdie, J. Martinez, J. L. Baneres, S. Mary, High constitutive activity is an intrinsic feature of ghrelin receptor protein: a study with a functional monomeric GHS-R1a receptor reconstituted in lipid discs. *J Biol Chem* **287**, 3630-3641 (2012); published online EpubFeb 3 (10.1074/jbc.M111.288324).

55. A. Kern, R. Albarran-Zeckler, H. E. Walsh, R. G. Smith, Apo-ghrelin receptor forms heteromers with DRD2 in hypothalamic neurons and is essential for anorexigenic effects of DRD2 agonism. *Neuron* **73**, 317-332 (2012); published online EpubJan 26 (10.1016/j.neuron.2011.10.038).

56. A. Kern, M. Mavrikaki, C. Ullrich, R. Albarran-Zeckler, A. F. Brantley, R. G. Smith, Hippocampal Dopamine/DRD1 Signaling Dependent on the Ghrelin Receptor. *Cell* **163**, 1176-1190 (2015); published online EpubNov 19 (10.1016/j.cell.2015.10.062).

57. E. J. Lopez Soto, F. Agosti, A. Cabral, E. R. Mustafa, V. M. Damonte, M. A. Gandini, S. Rodriguez, D. Castrogiovanni, R. Felix, M. Perello, J. Raingo, Constitutive and ghrelin-dependent GHSR1a activation impairs CaV2.1 and CaV2.2 currents in hypothalamic neurons. *The Journal of general physiology* **146**, 205-219 (2015); published online EpubSep (10.1085/jgp.201511383).

58. M. D. Valentina, R. S. Susana, R. Jesica, GHSR constitutive activity impairs voltage-gated calcium channel (CaV)-dependent inhibitory neurotransmission in hippocampal neurons. *J Physiol*, (2018); published online EpubSep 10 (10.1113/JP276256).

59. E. R. Mustafa, E. J. Lopez Soto, V. Martinez Damonte, S. S. Rodriguez, D. Lipscombe, J. Raingo, Constitutive activity of the Ghrelin receptor reduces surface expression of voltage-gated Ca(2+) channels in a CaVbeta-dependent manner. *Journal of cell science* **130**, 3907-3917 (2017); published online EpubNov 15 (10.1242/jcs.207886).

60. A. A. J. Rouault, L. K. Rosselli-Murai, C. C. Hernandez, L. E. Gimenez, G. G. Tall, J. A. Sebag, The GPCR accessory protein MRAP2 regulates both biased signaling and constitutive activity of the ghrelin receptor GHSR1a. *Science signaling* **13**, (2020); published online EpubJan 7 (10.1126/scisignal.aax4569).

61. M. Asai, S. Ramachandrappa, M. Joachim, Y. Shen, R. Zhang, N. Nuthalapati, V. Ramanathan, D. E. Strochlic, P. Ferket, K. Linhart, C. Ho, T. V. Novoselova, S. Garg, M. Ridderstrale, C. Marcus, J. N. Hirschhorn, J. M. Keogh, S. O'Rahilly, L. F. Chan, A. J. Clark, I. S. Farooqi, J. A. Majzoub, Loss of function of the melanocortin 2 receptor accessory protein 2 is associated with mammalian obesity. *Science* **341**, 275-278 (2013); published online EpubJul 19 (10.1126/science.1233000).

62. Genome-wide atlas of gene expression in the adult mouse brain. Available from http://mouse.brain-map.org/gene/show/89308.

63. Tissue-based map of the human proteome. Available from: https://www.proteinatlas.org/ENSG00000135324-MRAP2/brain.

64. A. Edwards, A. Abizaid, Clarifying the Ghrelin System's Ability to Regulate Feeding Behaviours Despite Enigmatic Spatial Separation of the GHSR and Its Endogenous Ligand. *International journal of molecular sciences* **18**, (2017); published online EpubApr 19 (10.3390/ijms18040859).

65. A. Cabral, E. J. Lopez Soto, J. Epelbaum, M. Perello, Is Ghrelin Synthesized in the Central Nervous System? *International journal of molecular sciences* **18**, (2017); published online EpubMar 15 (10.3390/ijms18030638).

66. S. Els, A. G. Beck-Sickinger, C. Chollet, Ghrelin receptor: high constitutive activity and methods for developing inverse agonists. *Methods Enzymol* **485**, 103-121 (2010)10.1016/B978-0-12-381296-4.00006-3).

67. S. W. Flavell, C. W. Cowan, T. K. Kim, P. L. Greer, Y. Lin, S. Paradis, E. C. Griffith, L. S. Hu, C. Chen, M. E. Greenberg, Activity-dependent regulation of MEF2 transcription factors suppresses excitatory synapse number. *Science* **311**, 1008-1012 (2006); published online EpubFeb 17 (10.1126/science.1122511).

68. M. Renner, D. Choquet, A. Triller, Control of the postsynaptic membrane viscosity. *J Neurosci* **29**, 2926-2937 (2009); published online EpubMar 4 (10.1523/JNEUROSCI.4445-08.2009).

69. S. D. Santos, O. Iuliano, L. Ribeiro, J. Veran, J. S. Ferreira, P. Rio, C. Mulle, C. B. Duarte, A. L. Carvalho, Contactin-associated protein 1 (Caspr1) regulates the traffic and synaptic content of alpha-amino-3-hydroxy-5-methyl-4-isoxazolepropionic acid (AMPA)-type glutamate receptors. *J Biol Chem* **287**, 6868-6877 (2012); published online EpubFeb 24 (10.1074/jbc.M111.322909).

70. B. H. Gahwiler, M. Capogna, D. Debanne, R. A. McKinney, S. M. Thompson, Organotypic slice cultures: a technique has come of age. *Trends Neurosci* **20**, 471-477 (1997); published online EpubOct (10.1016/s0166-2236(97)01122-3).

71. M. Jiang, L. Deng, G. Chen, High Ca(2+)-phosphate transfection efficiency enables single neuron gene analysis. *Gene Ther* **11**, 1303-1311 (2004); published online EpubSep (10.1038/sj.gt.3302305).

72. P. Opazo, S. Labrecque, C. M. Tigaret, A. Frouin, P. W. Wiseman, P. De Koninck, D. Choquet, CaMKII triggers the diffusional trapping of surface AMPARs through phosphorylation of stargazin. *Neuron* **67**, 239-252 (2010); published online EpubJul 29 (10.1016/j.neuron.2010.06.007).

73. L. Groc, M. Heine, L. Cognet, K. Brickley, F. A. Stephenson, B. Lounis, D. Choquet, Differential activity-dependent regulation of the lateral mobilities of AMPA and NMDA receptors. *Nat Neurosci* **7**, 695-696 (2004); published online EpubJul (10.1038/nn1270).

74. C. R. Gerfen, M. A. Rogawski, D. R. Sibley, P. Skolnick, S. Wray, *Short protocols in neuroscience: systems and behavioral methods*. M. A. R. E. Charles R. Gerfen (Editor), David R. Sibley (Editor), Phil Skolnick (Editor), Susan Wray (Editor), Ed., (John Wiley & Sons, 2006).

75. N. Matsuo, K. Takao, K. Nakanishi, N. Yamasaki, K. Tanda, T. Miyakawa, Behavioral profiles of three C57BL/6 substrains. *Frontiers in behavioral neuroscience* **4**, 29 (2010)10.3389/fnbeh.2010.00029).

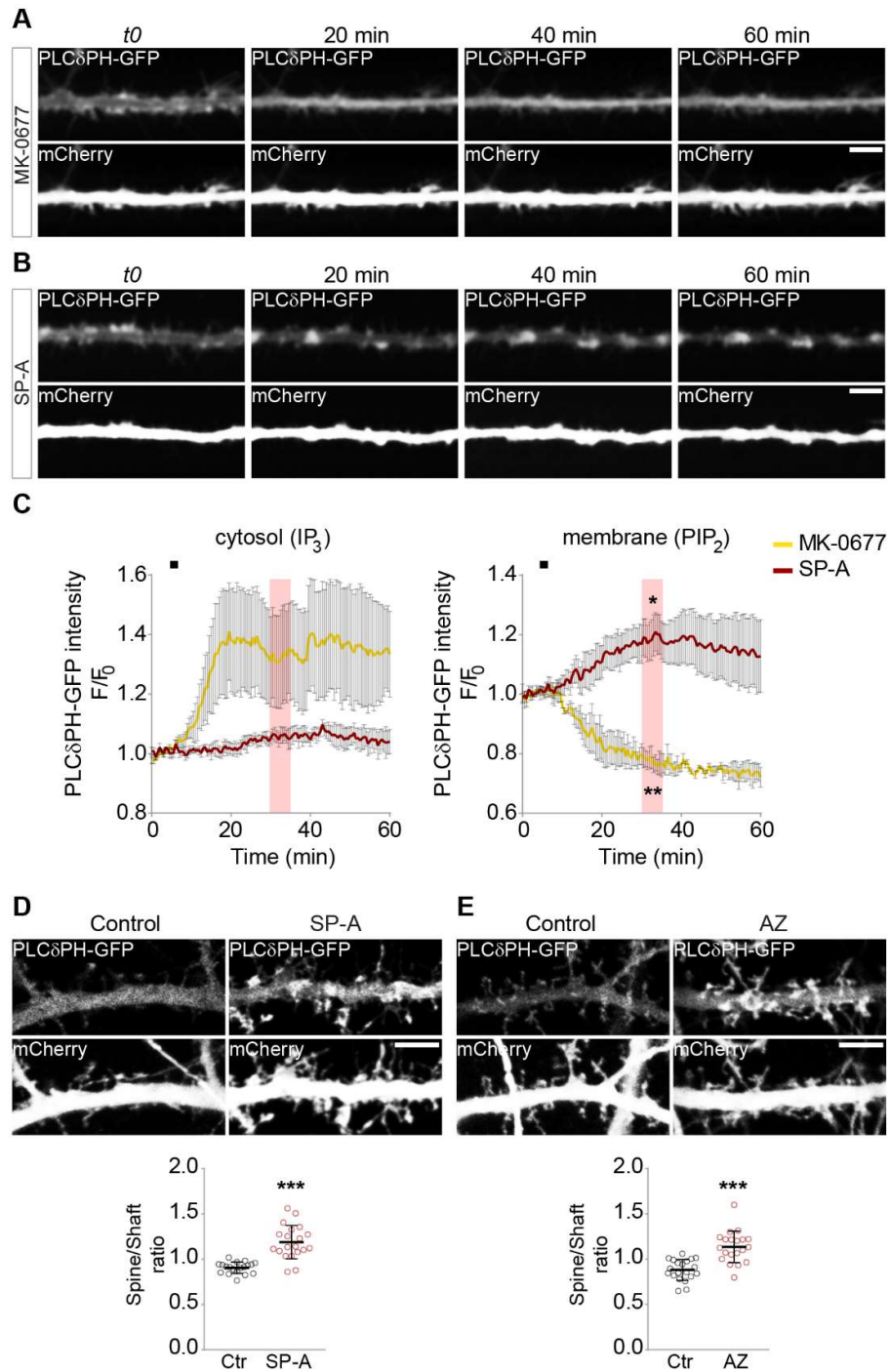**Figures and Figure legends**

Fig. 1

Fig. 1. Ligand-independent activity of GHS-R1a regulates PIP$_2$ hydrolysis in hippocampal cultured neurons.

(**A to C**) Analysis of hippocampal neurons co-transfected with PLCδPH-GFP and mCherry (DIV 13-14) then imaged for 60 min on DIV 15-16 upon application (at t=6 min, ■ in the graph) with either GHS-R1a agonist MK-0677 (1 μM, n = 4 neurons; A and C) or inverse agonist SP-A (1 μM, n = 5 neurons; B and C). Scale bars, 5 μm. Data are mean ± SEM PLCδPH-GFP fluorescence (F/F$_0$) in the dendritic cytoplasm and membrane, in 3 independent experiments. Differences in the 30 to 35.5 min period (pink) to the baseline (0 to 5.5 min) assessed by paired t-test, *P=0.0466 and **P=0.0071 (cytosol_MK: t = 2.104 and df = 3; cytosol_SP-A: t = 1.905 and df = 4; membrane_MK: t = 6.599 and df = 3; membrane_SP-A: t = 2.846 and df = 4). See also movies S1 and S2. (**D and E**) Imaging of DIV 15 hippocampal neurons that were co-transfected at DIV 13 with PLCδPH-GFP and mCherry and incubated at DIV 14 with SP-A (D; 1 μM) or AZ12861903 (E; AZ, 50 nM) for 20 hours. Scale bars, 5 μm. Data are mean (± SD) GFP intensity in spine heads relative to dendritic shaft (spine/shaft ratio) from 2 independent experiments, 19 to 20 neurons each condition. ***P < 0.0001 by unpaired t-test (t = 5.45 and df = 38).
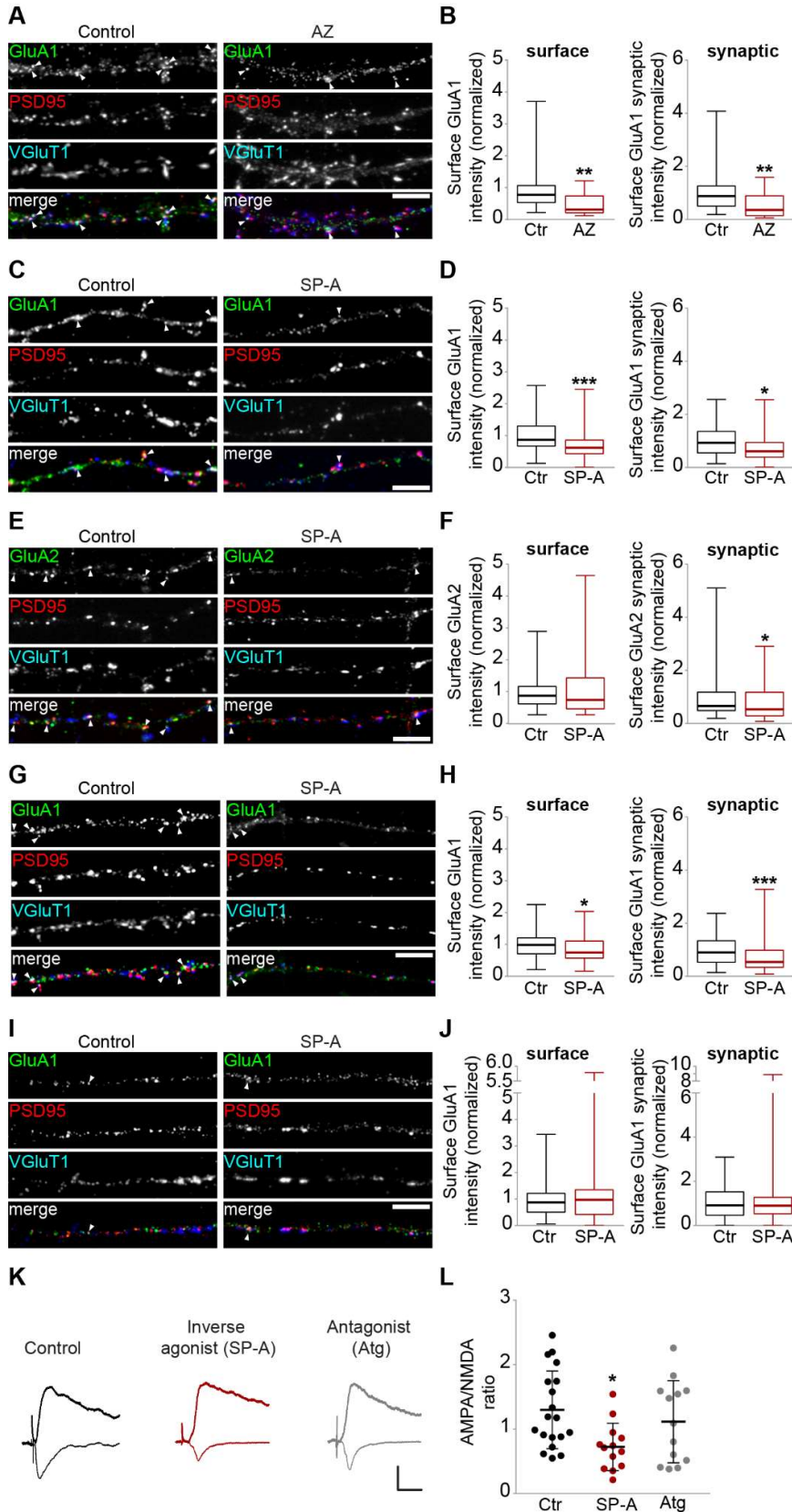
Fig. 2

Fig. 2. Ligand-independent activity of GHS-R1a controls synaptic levels of AMPARs and excitatory synaptic transmission in the hippocampus.

(**A to J**) Representative images and quantitative analysis of 7 (I), 15 (A, C and E) or 20 DIV (G) hippocampal neurons incubated with AZ 50 nM (A) or SP-A 1 µM (C, E, G and I) for 20 hours and immunostained for surface GluA1 or GluA2 (green), PSD95 (red) and VGluT1 (blue). Total fluorescence intensity of GluA1 or GluA2 cell-surface puncta (left) and total fluorescence intensity of GluA1 or GluA2 synaptic clusters (VGluT1/PSD95-colocalized, right) normalized to synapse density. Results are expressed as the median relative to control cells from 2 or 4 (B or D), 4 (F), 5 (H) and 4 (J) independent experiments. B, left and right (n = 24 neurons per group); D, left and right (Ctr, n = 60; SP-A, n = 59); F, left (n = 60) and right (n = 59) per group; H, left (n = 74 per group) and right (Ctr, n = 75; SP-A, n = 74); H, left (n = 74 per group) and right (Ctr, n = 75; SP-A, n = 74). Differences between groups were assessed by Mann-Whitney test (U = 138, 133, 1142, 1303, 1672, 1356, 2158, 1894, 1772 and 1695, respectively; and **P = 0.0016, **P = 0.0011, ***P = 0.0007, *P = 0.0128, P = 0.5047, *P = 0.0384, *P = 0.0260, ***P = 0.0007, P = 0.8857 and P = 0.8093, respectively). Scale bars, 5 µm. Arrowheads indicate synaptic GluA1- or GluA2-AMPARs (**K and L**) Representative traces and quantitative analysis of evoked synaptic AMPARs and NMDARs currents in 7 DIV organotypic hippocampal slices in control condition and upon treatment for 20 hours with SP-A 1 µM or [D-Lys3]-GHRP-6 (Atg) 100 µM. Scale bars: vertical, 50 pA; horizontal, 20 ms. AMPA/NMDA ratios are expressed as mean (± SD); Ctr (n = 19 neurons), SP-A (n = 13) and Atg (n = 13); 1-way ANOVA followed by Dunnett's multiple comparison test (F = 4.158 and *P = 0.0121). See also fig. S1.

Fig. 3

A
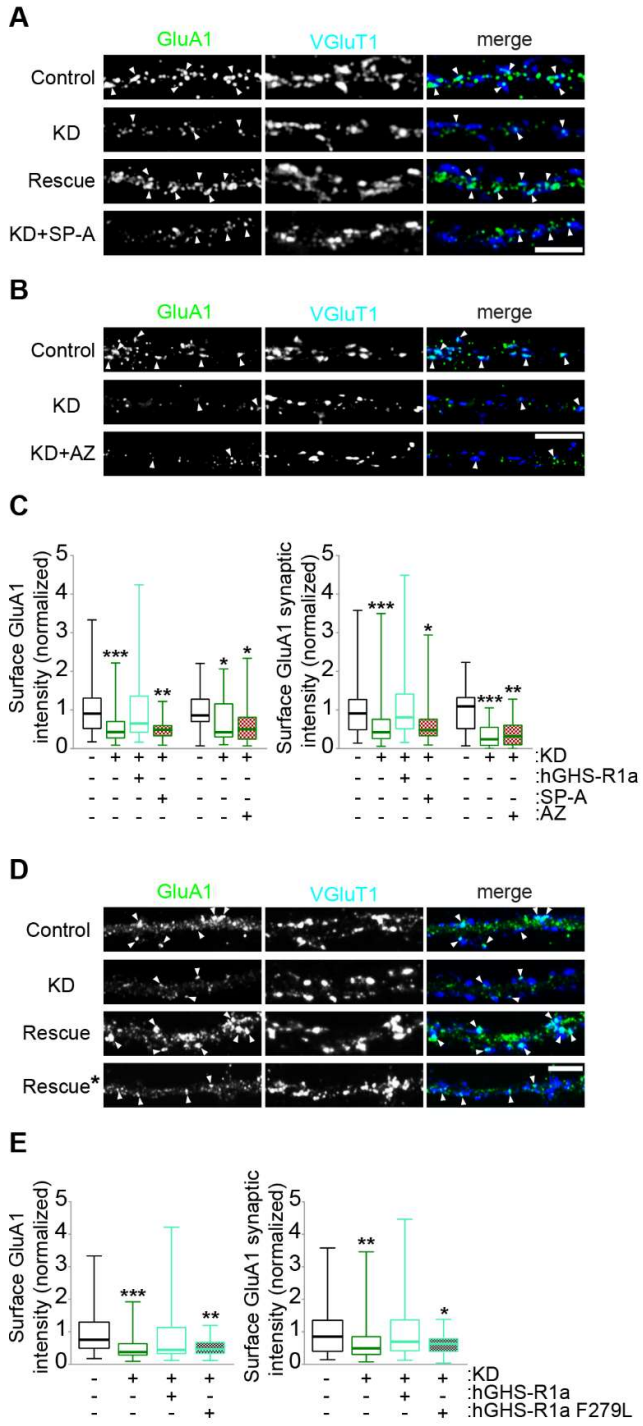

B

C

D

E

Fig. 3. Inverse agonists AZ12861903 and SP-A specifically target GHS-R1a to control synaptic levels of AMPARs.

(**A, B and D**) Representative images of 15 DIV hippocampal neurons transfected with constructs encoding luciferase shRNA-GFP (control), GHS-R1a shRNA-GFP (KD), GHS-R1a shRNA-GFP + hGHS-R1a (rescue) or GHS-R1a shRNA-GFP + hGHS-R1a F279L (rescue*). Neurons expressing GHS-R1a shRNA-GFP were treated with SP-A 1 µM (A) or AZ 50 nM (B) for 20 hours. Neurons were immunostained for surface GluA1 (green) and VGluT1 (blue). Scale bars, 5 µm. Arrowheads indicate VGluT1-colocalized GluA1-AMPARs. (**C and E**) Quantitative analysis of total fluorescence intensity of GluA1 cell-surface puncta (left) and total fluorescence intensity of GluA1 synaptic clusters (VGluT1-colocalized, right) normalized to density of VGluT1 clusters. Results are expressed as the median relative to control cells from 2 to 4 (C) and 3 or 4 (E) independent experiments. Differences between groups: left_SP-A (Ctr, $n = 51$ neurons; KD, $n = 50$; rescue, $n = 51$; KD + SP-A, $n = 36$), left_AZ (Ctr, $n = 22$; KD, $n = 21$; KD + AZ, $n = 21$), right_SP-A (Ctr, $n = 51$; KD, $n = 51$; rescue, $n = 52$; KD + SP-A, $n = 36$) and right_AZ (Ctr, $n = 22$; KD, $n = 20$; KD + AZ, $n = 22$) (C), and left (Ctr, $n = 54$; KD, $n = 52$; rescue, $n = 54$; rescue*, $n = 39$) and right (Ctr, $n = 53$; KD, $n = 52$; rescue, $n = 54$; rescue*, $n = 37$) (E) were assessed by Kruskal-Wallis analysis of variance followed by Dunn's multiple comparison test (Kruskal-Wallis statistic = 26.2, 7.899, 23.64, 17.65, 20.09 and 14,79, respectively; and ***$P < 0.0001$, **$P = 0.0059$, *$P = 0.0447$, *$P = 0.0219$, ***$P = 0.0004$, *$P = 0.0336$, ***$P = 0.0003$, **$P = 0.0010$, ***$P < 0.0001$, **$P = 0.0070$, **$P = 0.0018$ and *$P = 0.0358$).
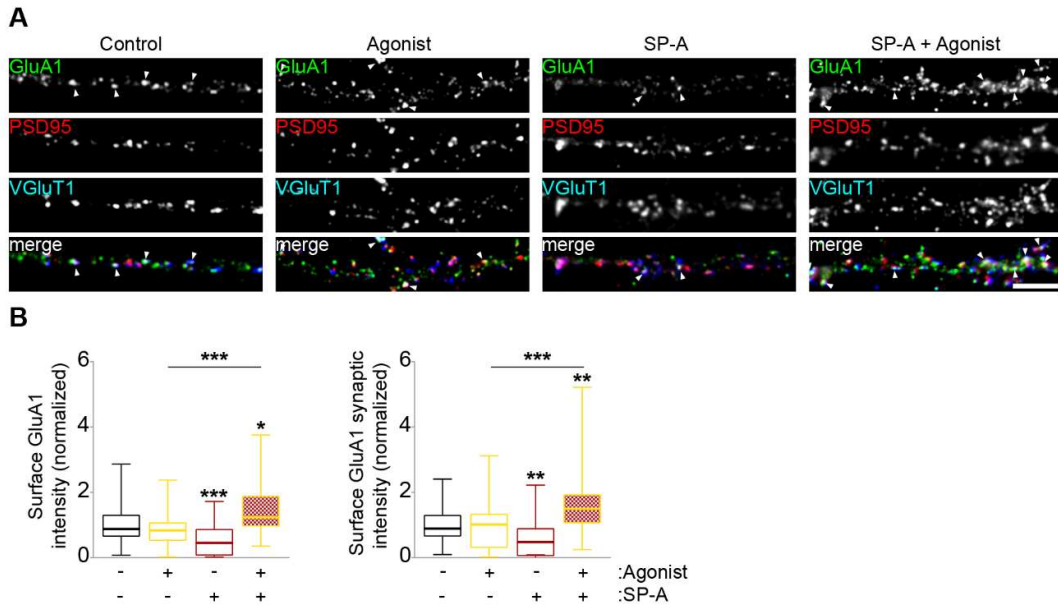
Fig. 4

Fig. 4. **Incubation with the GHS-R1a inverse agonist [D-Arg[1],D-Phe[5],D-Trp[7,9],Leu[11]]-substance P enhances GHS-R1a agonist MK-0677-induced effect on synaptic levels of AMPARs.**

(**A**) Representative images of 15 DIV hippocampal neurons incubated with MK-0677 1 μM for 1 hour, with the inverse agonist SP-A 1 μM for 15 min or with the SP-A for 15 min followed by MK-0677 for 1 hour. Neurons were immunostained for surface GluA1 (green), PSD95 (red) and VGluT1 (blue). Scale bar, 5 μm. Arrowheads indicate synaptic GluA1-AMPARs. (**B**) Quantitative analysis of total fluorescence intensity of GluA1 cell-surface puncta (left) and total fluorescence intensity of GluA1 synaptic clusters (VGluT1/PSD95-colocalized, right) normalized to synapse density. Results are expressed as the median relative to control cells from 3 or 5 independent experiments. Differences between groups: left and right (Ctr and agonist, n = 75 neurons; SP-A and SP-A + agonist, n = 45) were assessed by Kruskal-Wallis analysis of variance followed by Dunn's multiple comparison test (Kruskal-Wallis statistic = 48.21 and 42.65, respectively; and ***P < 0.0001, *P = 0.0110, **P = 0.0014, **P = 0.0018 and ***P = 0.0005).
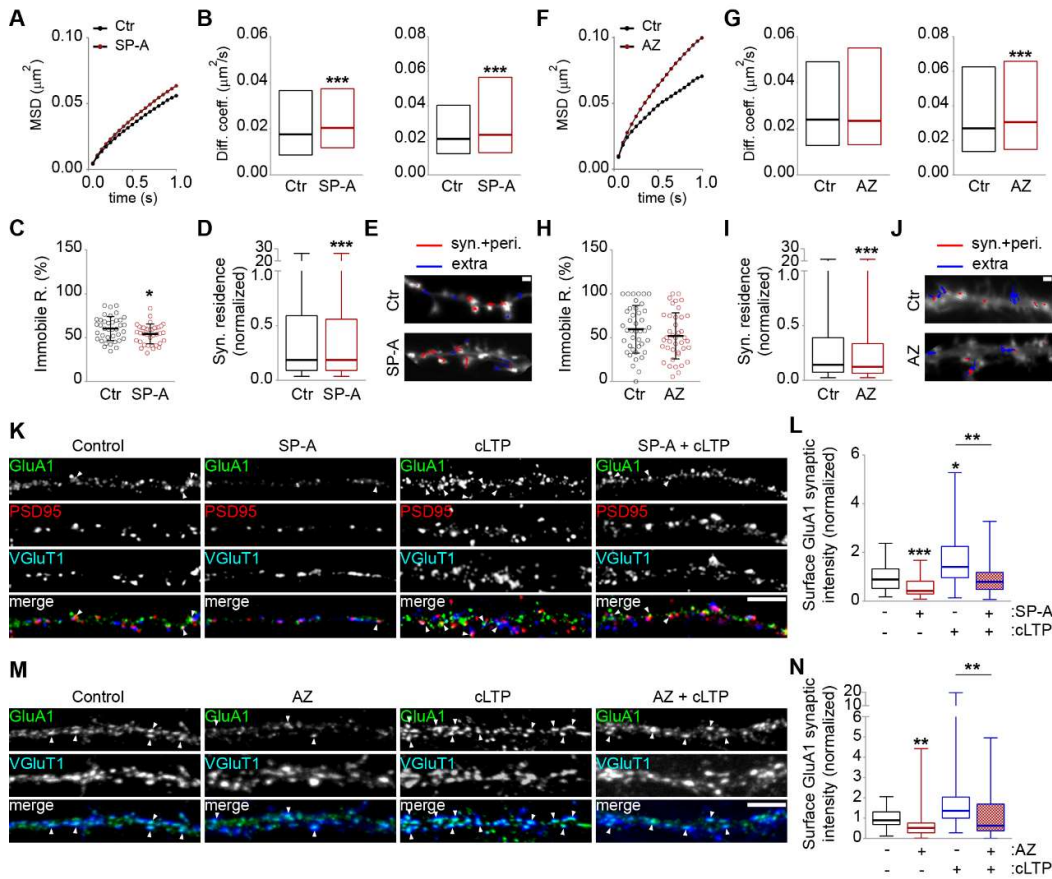
Fig. 5

Fig. 5. Blockage of the ligand-independent activity of GHS-R1a increases the cell surface diffusion of AMPARs, and prevents the activity-triggered delivery of AMPARs to synaptic sites.

(**A to E**) Single particle tracking analysis of SEP-GluA1 in 15 DIV hippocampal neurons co-transfected with SEP-GluA1 and Homer1C-DsRed (at 11 DIV) and incubated with SP-A 1 µM for 1 hour by using quantum dots labelled antibodies for GFP (QD-GluA1). GluA1 mean square displacement (MSD) versus time plots for control and SP-A-treated cells (A). Surface diffusion coefficient of synaptic (left) and global (right) single QD-GluA1. Median diffusion (± 25%–75% IQR) of 8816–8607 trajectories; Mann-Whitney test (U = 803490 and 17834511, respectively; and ***P < 0.0001) (B). Mean percentage (± SD) of synaptic immobile GluA1-AMPARs in control and SP-A-treated cells. Ctr (n = 38 neurons) and SP-A (n = 37); unpaired t-test (t = 2.113, df = 73 and *P = 0.0380) (C).

Synaptic residence time (median) of GluA1-AMPARs in control and SP-A-treated cells. Mann-Whitney test (U = 1799767896 and ***P < 0.0001) (D). Reconstructed GluA1 trajectories in the synaptic (red) and extrasynaptic compartments (blue). A minimum of 37 cells were analyzed in 3 independent experiments. Scale bar, 1 µm (E). (**F to J**) Single particle tracking analysis of GluA1 in 15 DIV hippocampal neurons transfected with Homer1C-DsRed (at 11 DIV) and incubated with AZ 50 nM for 1 hour by using quantum dots-labelled antibodies for GluA1 (QD-GluA1). GluA1 mean square displacement (MSD) versus time plots for control and AZ-treated cells (F). Surface diffusion coefficient of synaptic (left) and global (right) single QD-GluA1. Median diffusion (± 25%–75% IQR) of 1770–1303 trajectories; Mann-Whitney test (U = 15250 and 212277, respectively; and P = 0.7338 and ***P < 0.0001, respectively) (G). Mean percentage (± SD) of synaptic immobile GluA1-AMPARs in control and AZ-treated cells. Ctr (n = 41 neurons) and AZ (n = 40); unpaired t-test (t = 1.269, df = 79 and P = 0.2081) (H). Synaptic residence time (median) of GluA1-AMPARs in control and AZ-treated cells. Mann-Whitney test (U = 39940707 and ***P < 0.0001) (I). Reconstructed GluA1 trajectories in the synaptic (red) and extrasynaptic compartments (blue). A minimum of 40 cells were analyzed in 3 independent experiments. Scale bar, 1 µm (J). See also fig. S2. (**K to N**) Representative images and quantitative analysis of 19–20 DIV hippocampal neurons treated with SP-A 1 µM (K) or AZ 50 nM (M) for 20 hours, submitted to cLTP or pre-treated with SP-A (K) or AZ (M) and submitted to cLTP. Neurons were immunostained for surface GluA1 (green), PSD95 (red) and VGluT1 (blue) (K) or surface GluA1 (green) and VGluT1 (blue) (M). Scale bar, 5 µm. Arrowheads indicate synaptic GluA1-AMPARs (K) or VGluT1-colocalized GluA1-AMPARs (M). Total fluorescence intensity of GluA1 synaptic clusters (VGluT1/PSD95-colocalized) (K) or (VGluT1-colocalized) (M) normalized to synapse density or VGluT1 clusters, respectively. Data are median relative to control cells from 3 or 4 (L) or 3 (N) independent experiments. Ctr (n = 60 neurons), SP-A (n = 59), cLTP (n = 44) and SP-A + cLTP (n = 43); Ctr (n = 39),

AZ, cLTP and AZ + cLTP (n = 40); Kruskal-Wallis analysis of variance followed by Dunn's multiple comparison test (Kruskal-Wallis statistic = 44.11 and 35.87, respectively; and ***P = 0.0004, *P = 0.0259, **P = 0.0018, **P = 0.0021 and **P = 0.001.
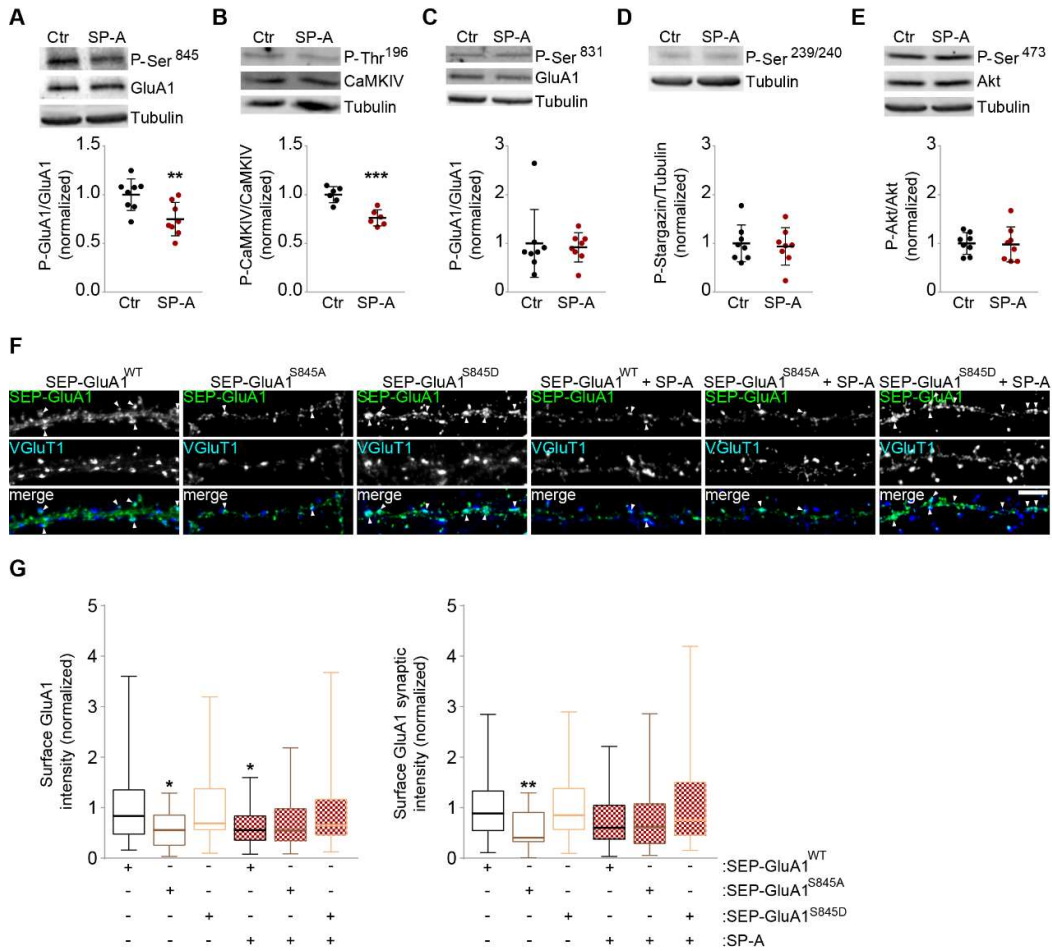
Fig. 6

A   Ctr SP-A
P-Ser^{845}
GluA1
Tubulin

B   Ctr SP-A
P-Thr^{196}
CaMKIV
Tubulin

C   Ctr SP-A
P-Ser^{831}
GluA1
Tubulin

D   Ctr SP-A
P-Ser$^{239/240}$
Tubulin

E   Ctr SP-A
P-Ser^{473}
Akt
Tubulin

F

SEP-GluA1^{WT} SEP-GluA1^{S845A} SEP-GluA1^{S845D} SEP-GluA1^{WT} + SP-A   SEP-GluA1^{S845A} + SP-A   SEP-GluA1^{S845D} + SP-A

G

Fig. 6. Signaling pathways downstream of the ligand-independent GHS-R1a activity.

(**A to E**) Western blot analysis of 7 DIV organotypic hippocampal slices non-treated or treated with SP-A 1 µM for 20 hours. Primary antibodies detected: phospho-Ser^{845} at GluA1 (A), phospho-Thr^{196} at CaMKIV (B), phospho-Ser^{831} at GluA1 (C), phospho-Ser$^{239/240}$ at stargazin (D), phospho-Ser^{473} at Akt, total GluA1 (A, C), total CaMKIV (B) and total Akt (E). Tubulin was used as a loading control. The graphs represent the quantification of band intensities (mean ± SD) relative to control extracts in 8 (A and C to E) or 6 (B) independent experiments. The statistical significance was calculated using the unpaired t-test: Ser^{845} (t = 3.011, df = 14 and **P = 0.0093), Thr^{196} (t = 5.012, df = 10

and ***P = 0.0005), Ser^{831} (t = 0.3006, df = 14 and P = 0.7681), Ser$^{239/240}$ (t = 0.3211, df = 14 and P = 0.7529) and Ser^{473} (t = 0.1313, df = 14 and P = 0.8974). (**F and G**) Representative images and quantitative analysis of 15 DIV hippocampal neurons expressing SEP-GluA1^{WT}, SEP-GluA1^{S845A} or SEP-GluA1^{S845D} (non-treated or treated with SP-A 1 µM for 20 hours). Neurons were immunostained for surface GFP (green) and VGluT1 (blue). Scale bar, 5 µm. Arrowheads indicate VGluT1-colocalized GluA1-AMPARs. Total fluorescence intensity of SEP-GluA1 cell-surface puncta (left) and total fluorescence intensity of SEP-GluA1 synaptic clusters (VGluT1-colocalized, right) normalized to density of VGluT1 clusters. Data are median relative to control cells from 3 independent experiments. Differences between groups: left (WT and S845A , n = 39 neurons; S845D, n = 37; WT + SP-A, n = 38; S845A + SP-A, n = 37; S845D + SP-A, n = 38) and right (WT and S845A, n = 39; S845D and WT + SP-A, n = 38; S845A + SP-A, n = 37; S845D + SP-A, n = 39) were assessed by Kruskal-Wallis analysis of variance followed by Dunn's multiple comparison test (Kruskal-Wallis statistic = 14.87 and 16.29, respectively; and *P = 0.0158 and **P = 0.0072).
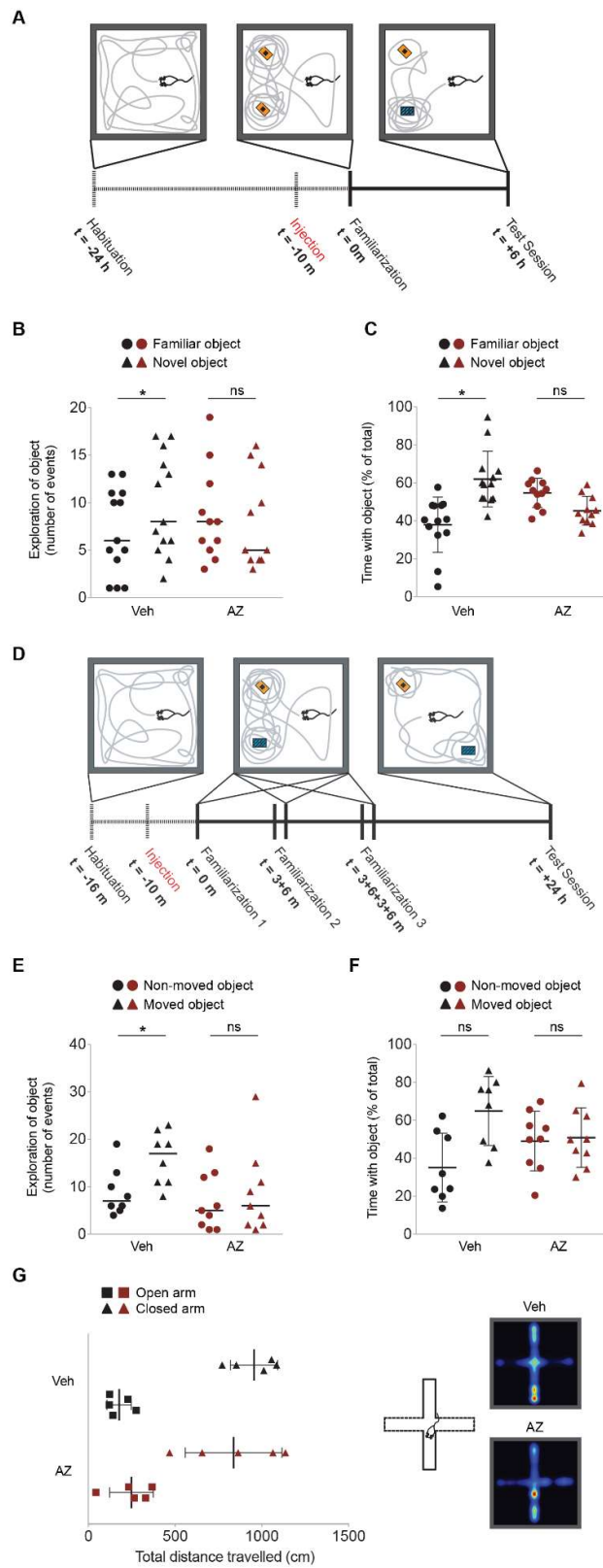
Fig. 7

Fig. 7. Administration of an inverse agonist of GHS-R1a impairs recognition and spatial memory.

(**A to C**) Male C57/BL6 mice of 8-15 weeks of age received intraperitoneal (i.p.) injections of 100 mg/kg of AZ or Vehicle and undergone the novel object recognition test. (**A**) Schematic representation of a novel object recognition test with the "habituation", "drug injection", "familiarization" and "test session" time line (described in detail in the methods section). (**B**) Number of interactions with objects during test session expressed as a percentage of the total of interactions with both objects during test session (median). Differences between groups (Veh, n = 13; AZ, n = 11) were assessed by Wilkoxon matched-pairs signed rank test: Old vs Novel object in Veh and AZ group (*P = 0.0303 and P = 0.3945, respectively). (**C**) Time spent interacting with objects during the test session expressed as a percentage of total duration of interactions with both objects (mean ± SD). Differences between groups were assessed using the paired t-test: Old vs Novel object in Veh group (t = 2.968, df = 12, *P = 0.0117) and AZ group (t= 2.04, df = 10, P = 0.0686). (**D to F**) Male C57/BL6 mice of 8-15 weeks of age received (i.p.) injections of 100 mg/kg of AZ or Vehicle and underwent the object displacement recognition test. (**D**) Schematic representation of an object displacement recognition test with "habituation", "drug injection", "familiarization" and "test session" time line (Described in detail in the methods section). (**E**) Number of interactions with objects during test session expressed as a percentage of all interactions with objects (median). Comparison between groups (Veh, n = 8; AZ n = 9) was assessed using the Wilkoxon matched-pairs signed rank test: Non-moved vs Moved object in Veh group (*P = 0.0469) and AZ group (P = 0.3438). (**F**) Time spent with objects during the test session is expressed as a percentage of total duration of interaction with both objects (mean ± SD). Comparisons between groups (Veh, n = 8; AZ, n = 9) were assessed using the paired t-test: Non-moved vs Moved object in Veh group (t = 2.325, df = 7, P = 0.053) and AZ group (t = 0.1798, df = 8, P = 0.8618). (**G**) **A**nimals received (i.p.) injections of 100 mg/kg

of AZ or Vehicle and underwent the elevated plus maze test. Distance travelled in the maze (cm, mean ± SD) was assessed to evaluate anxiety-like behavior. Differences between groups (Veh, n = 5; AZ, n = 5) were assessed using unpaired t-test: comparisons for closed arms (t = 1.085, df = 8, P = 0.4209) and open arms (t = 1.085, df = 8, P = 0.3095). Schematic of elevated plus maze and heatmaps representing cumulative time spent in each part of the maze by each group (Veh and AZ). Additional data in fig. S3.
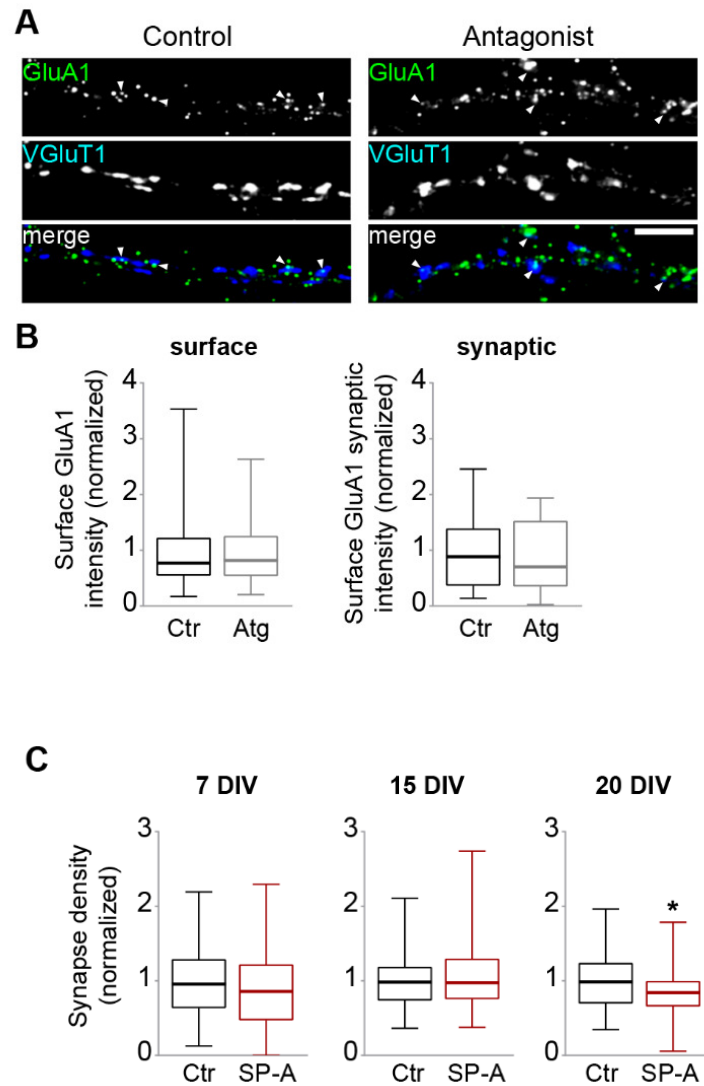
Figure S1. Blockage of the ligand-independent activity of GHS-R1a decreases the synapse density in mature primary cultured hippocampal neurons. (A) Hippocampal neurons at 15 days in vitro (15 DIV) were incubated with GHS-R1a antagonist JMV2959 (100 µM for 20 hours) and immunostained for surface GluA1 (green) and VGluT1 (blue) under non-permeabilizing conditions. Scale bar, 5 µm. Arrowheads indicate VGluT1-colocalized GluA1-AMPARs. **(B)** Quantification of data described in (A): total fluorescence intensity of GluA1 cell-surface puncta (surface) and total fluorescence intensity of GluA1 synaptic clusters (VGluT1-colocalized), normalized to density of VGluT1 clusters. Ctr, control; Atg, antagonist. Results are shown as the median relative to control cells from 2 independent experiments (each condition, n = 22 neurons), compared by the Mann-Whitney test: U = 239 and 222, respectively; P = 0.9537 and 0.6503, respectively. **(C)** 7 DIV, 15 DIV and 20 DIV hippocampal neurons were incubated with GHS-R1a inverse agonist SP-A (1 µM for 20 hours) and analyzed for synapse density inferred from PSD95- and VGluT1-positive puncta. Results are shown as the median relative to control cells from 4 or 5 independent experiments (each condition, n = 60 neurons at 7 and 15 DIV, 75 neurons at 20 DIV), and compared by Mann-Whitney test: U = 1592, 1778 and 2221, respectively; and *P = 0.2772, 0.9105 and 0.0260, respectively. Data are related to those in Fig. 2.
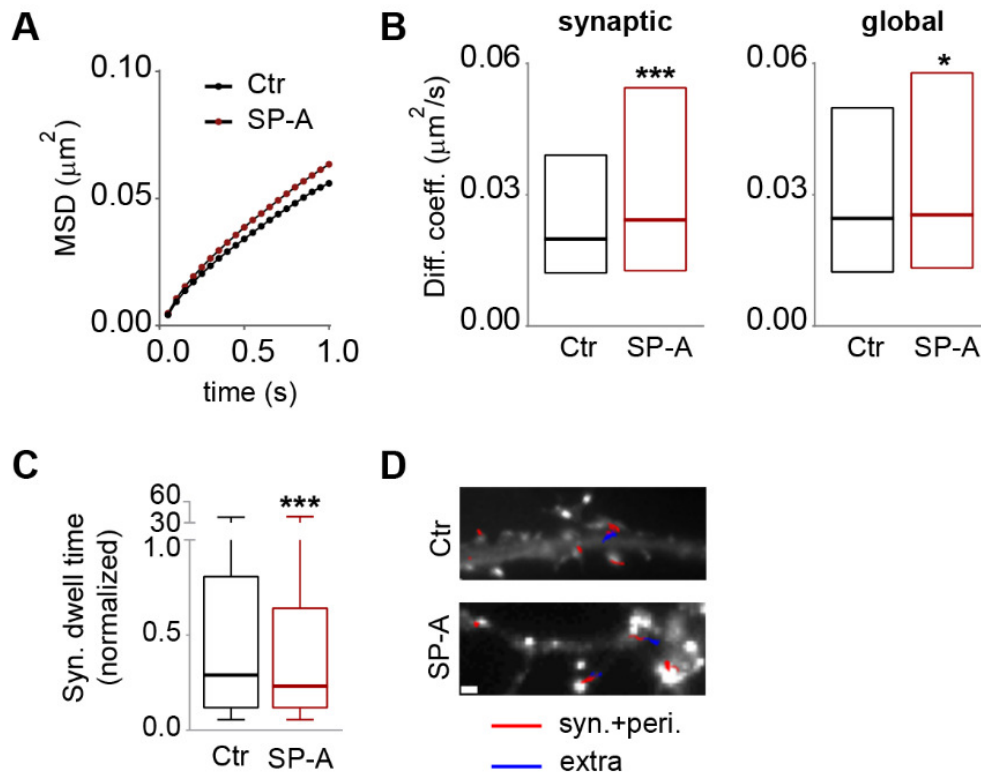
Figure S2. Blockade of the ligand-independent activity of GHS-R1a increases the cell surface diffusion of GluA2-AMPARs. (A to D) Hippocampal neurons transfected with Homer1C-GFP at 11 DIV were either untreated (Ctr) or incubated with SP-A (1 µM) for 1 hour at 15 DIV prior to assessing GluA2 surface diffusion using quantum dots-labelled antibody for GluA2 (QD-GluA2). Shown are (A) the GluA2 mean square displacement (MSD) versus time; (B) the surface diffusion coefficient of synaptic (left) and global (right) single QD-GluA2; (C) the median synaptic dwell time of GluA2; and (D) representative, reconstructed GluA2 trajectories in the synaptic and extrasynaptic compartments (red and blue, respectively), each in control and SP-A–treated cells. Scale bar (D), 1 µm. A minimum of 33 cells and 4356-2288 trajectories were analyzed in 3 independent experiments. Data were compared by Mann-Whitney tests: U = 8807 and 927240, respectively in (B), and U = 17648853 in (C); *$P < 0.05$ ($P = 0.0122$) and ***$P < 0.0001$. Data are related to those in Fig. 5.
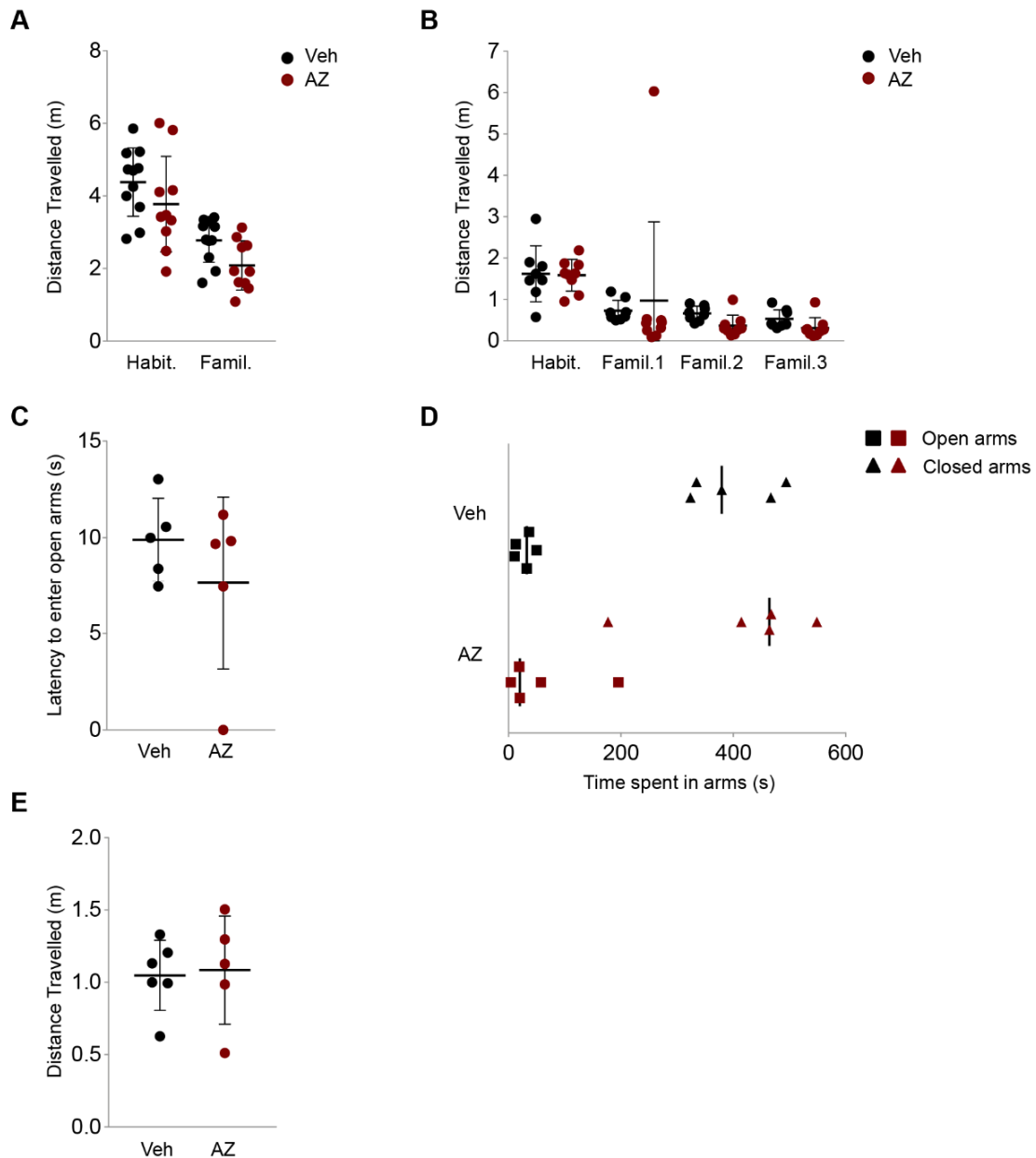
Figure S3. Administration of an inverse agonist of GHS-R1a does not impair overall movement. (A and B) Male C57/BL6 mice of 8-15 weeks of age received intraperitoneal (i.p.) injections of 100 mg/kg AZ or Vehicle and performed novel object recognition and object displacement recognition tests. (**A**) Distance travelled (mean ± SD) by each animal in the novel object recognition "habituation" and "familiarization" sessions. Comparisons between groups (Veh, $n = 11$; AZ $n = 10$) were evaluated by two-way ANOVA and Bonferroni correction for multiple comparisons: variation by session [F(1,19) = 46.6 and ***P < 0.0001] interaction [F(1,19) = 0.03185 and P = 0.8602], and treatment [F(1,19) = 4.093 and P = 0.0574], and multiple comparisons test between groups for habituation (P = 0.2782) and familiarization (P = 0.1853). (**B**) Distance travelled (mean ± SD) by each animal in the object displacement recognition "habituation" and "familiarization" sessions. Comparisons between groups (Veh, $n = 8$; AZ $n = 9$) were evaluated by two-way ANOVA and Bonferroni correction for multiple comparisons: variations by session [F(3,45) = 7.903 and P = 0.0002] interaction [F(3,45) = 0.3985 and P = 0.7547] and treatment [F(1,15) = 0.1948 and P = 0.6652], and multiple comparisons test between groups for habituation (P > 0.9999) familiarization 1 (P > 0.9999) familiarization 2 (P > 0.9999) familiarization 3 (P > 0.9999). **(C to E)** Animals of

3

8-15 weeks underwent the elevated plus maze test. Behavior was evaluated by (**C**) latency to enter open arms (s, mean ± SD), (**D**) time spent on each arm (median), and (**E**) total movement (cm, mean ± SD). Comparisons between groups (Veh, n = 5; AZ, n = 5) for latency to enter open arms (C) and median time spent on each arm (E) was assessed using unpaired t-tests: t = 1.016, df = 8, and P = 0.3396; t = 0.2654, df = 8 and P = 0.7974, respectively. Comparison between groups total movement (D) was evaluated using the Mann-Whitney test: closed arms: U = 10 and P = 0.6905; open arms: U = 11 and P = 0.8413. Data are related to those in Fig. 7.

SUPPLEMENTAL MATERIAL

Movie S1. Application of the GHS-R1a agonist MK-0677 induces the translocation of PLCδPH-GFP from the plasma membrane into the cytosol. Spinning disk confocal live cell imaging of DIV15 WT rat hippocampal neuron co-expressing mCherry (not shown) and PLCδPH-GFP. The cell was imaged every 30 s, for a total period of 60 min. MK-0677 (1 μM) was added at 6 min. Frame Rate: 15 fps. Scale bar: 10 μm

Movie S2. Application of the GHS-R1a inverse agonist SP-A increases the plasma membrane levels of PLCδPH-GFP. Spinning disk confocal live cell imaging of DIV15 WT rat hippocampal neuron co-expressing mCherry (not shown) and PLCδPH-GFP. The cell was imaged every 30 s, for a total period of 60 min. SP-A (1 μM) was added at 6 min. Frame Rate: 15 fps. Scale bar: 10 μm